AD-A173 447 A NEW EFFICIENT FORMULATION FOR THIN SHELL FINITE ELEMENT MODELS(U) MARYLAND UNIV COLLEGE PARK DEPT OF AEROSPACE ENGINEERING J J RHIU ET AL. 14 OCT 86 1/1

UNCLASSIFIED N00014-84-K-0385 F/G 22/2 NL

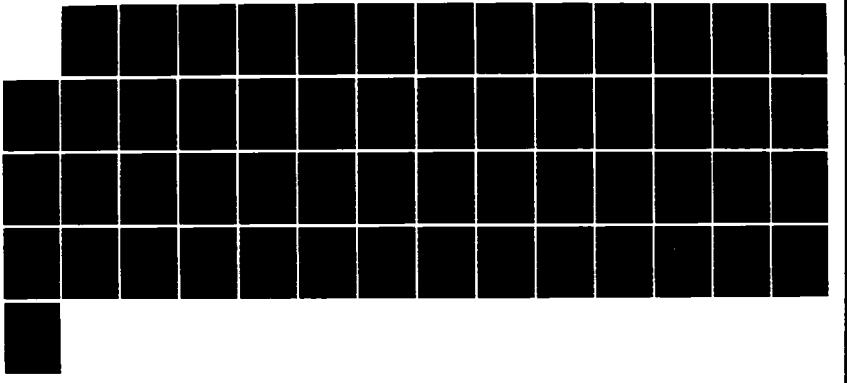

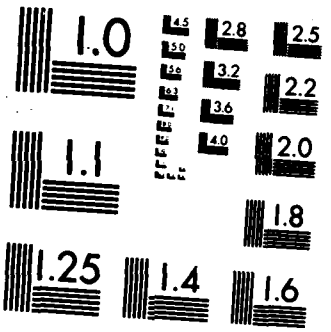

A NEW EFFICIENT FORMULATION FOR THIN SHELL FINITE ELEMENT MODELS

J.J. RHIU

S.W. LEE

October 1986

INTERIM REPORT

Office of Naval Research
Contract No. N00014-84-K-0385
Work Unit No. 4324-718

AD-A173 447

REPORT DOCUMENTATION PAGE

1a. REPORT SECURITY CLASSIFICATION: Unclassified	1b. RESTRICTIVE MARKINGS
2a. SECURITY CLASSIFICATION AUTHORITY	3. DISTRIBUTION/AVAILABILITY OF REPORT: Unlimited
2b. DECLASSIFICATION/DOWNGRADING SCHEDULE	
4. PERFORMING ORGANIZATION REPORT NUMBER(S)	5. MONITORING ORGANIZATION REPORT NUMBER(S)
6a. NAME OF PERFORMING ORGANIZATION: Department of Aerospace Eng. University of Maryland; 6b. OFFICE SYMBOL (If applicable)	7a. NAME OF MONITORING ORGANIZATION: Office of Naval Research Mechanics Division
6c. ADDRESS (City, State and ZIP Code): College Park, Maryland 20742	7b. ADDRESS (City, State and ZIP Code): 800 North Quincy Street Arlington, Virginia 22217
8a. NAME OF FUNDING/SPONSORING ORGANIZATION: Office of Naval Research; 8b. OFFICE SYMBOL (If applicable)	9. PROCUREMENT INSTRUMENT IDENTIFICATION NUMBER: N00014-84-K-0385
8c. ADDRESS (City, State and ZIP Code): 800 North Quincy Street Arlington, Virginia 22217	10. SOURCE OF FUNDING NOS.

PROGRAM ELEMENT NO.	PROJECT NO.	TASK NO.	WORK UNIT NO.
			4324-718

11. TITLE (Include Security Classification): A New Efficient Formulation for Thin Shell Finite Element Models

12. PERSONAL AUTHOR(S): J.J. Rhiu and S.W. Lee

13a. TYPE OF REPORT	13b. TIME COVERED	14. DATE OF REPORT (Yr., Mo., Day)	15. PAGE COUNT
interim	FROM Oct. '85 TO Sept. '86	October 14, 1986	53

16. SUPPLEMENTARY NOTATION

17 COSATI CODES			18. SUBJECT TERMS (Continue on reverse if necessary and identify by block number)
FIELD	GROUP	SUB. GR.	shell finite element, stabilization scheme, new mixed formulation, Hellinger-Reissner principle, assumed strain

19. ABSTRACT (Continue on reverse if necessary and identify by block number)

A nine node shell element is developed by a new and more efficient mixed formulation. The new shell element formulation is based on the Hellinger-Reissner principle with independent strain and the concept of degenerate solid shell. The new formulation is made more efficient in terms of computing time than the conventional mixed formulation by dividing the assumed strain fields into a lower order part and a higher order part. Numerical results demonstrate that the present nine node element is free of locking even for very thin plates and shells and is also kinematically stable. In fact the stiffness matrix associated with the higher order assumed strain plays the role of a stabilization matrix.

20. DISTRIBUTION/AVAILABILITY OF ABSTRACT: UNCLASSIFIED/UNLIMITED ☐ SAME AS RPT. ☐ DTIC USERS ☐	21. ABSTRACT SECURITY CLASSIFICATION: Unclassified

22a. NAME OF RESPONSIBLE INDIVIDUAL	22b. TELEPHONE NUMBER (Include Area Code)	22c. OFFICE SYMBOL
Dr. R.E. Whitehead, Mechanics Division ONR	(202)696-4305	

DD FORM 1473, 83 APR — EDITION OF 1 JAN 73 IS OBSOLETE.

A NEW EFFICIENT FORMULATION FOR THIN SHELL FINITE ELEMENT MODELS

J.J. RHIU

S.W. LEE

October 1986

INTERIM REPORT

Office of Naval Research
Contract No. N00014-84-K-0385
Work Unit No. 4324-718

ABSTRACT

→ A nine node shell element is developed by a new and more efficient mixed formulation. The new shell element formulation is based on the Hellinger-Reissner principle with independent strain and the concept of degenerate solid shell. The new formulation is made more efficient in terms of computing time than the conventional mixed formulation by dividing the assumed strain fields into a lower part and a higher order part. Numerical results demonstrate that the present nine node element is free of locking even for very thin plates and shells and is also kinematically stable. In fact the stiffness matrix associated with the higher order assumed strain plays the role of a stabilization matrix. ←

INTRODUCTION

As far as the description of geometry and kinematics of deformation are concerned, the advent of degenerate solid shell element [1] represents an important milestone in the development of the finite element method for analysis of

thin shell structures. The degenerate solid shell concept adopts the basic assumptions in shell theory which allows transverse shear deformation and an isoparametric representation in the finite element approximation. As such it can be applied to finite element modeling of arbitrary shell geometries without resorting to a particular shell theory.

However, unless special care is taken, the performance of a degenerate solid shell element deteriorates rapidly as shell thickness becomes thinner. This undesirable phenomenon, called locking, reflects the inability of a shell element to represent zero inplane and transverse shear strain states without disrupting bending behavior [2].

In an attempt to alleviate the effect of locking, reduced/selective integration [3-9] has been widely used in conjunction with finite element models based on the displacement method. However, a reduced integration scheme does not necessarily guarantee a problem-free element. For example, 2x2 reduced integration rule applied to an eight node displacement model element is not capable of eliminating the locking effect completely. Moreover, as in the case of four node and nine node elements an excessively lower order of integration introduces unstable spurious kinematic modes or zero strain energy modes [8-10]. In order to suppress kinematic modes, a stabilization matrix can be added to the stiffness matrix evaluated by a reduced integration scheme [11,12].

Alternatively, Lee and Pian [2] showed that a mixed formulation based on the Hellinger-Reissner principle or a modified Hellinger-Reissner principle can be used to alleviate locking. In this formulation, an independent strain is assumed in terms of parameters within an element in addition to the usual assumed displacement. The assumed strain parameters are eliminated at element level. Of course, for an element with a given number of nodes, the degree of locking depends essentially on the choice of assumed strain. Moreover, a mixed formulation provides a rational mathematical basis for the reduced and selective

integration scheme [2, 13, 14,]. Following this approach, a nine node shell element with specific assumed inplane and transverse shear strains has been developed and applied to thin plates and shells [15, 16]. It has been found that this nine node element is free of locking and has no compatible or commutable spurious kinematic modes. However, in the conventional mixed formulation used in references 15 and 16, it is necessary to invert certain matrices in order to generate an element stiffness matrix. Therefore in comparison with the assumed displacement model based on the principle of virtual work, the conventional mixed formulation requires substantially more time to compute an element stiffness matrix of the same size.

In order to overcome this shortcoming of the conventional mixed formulation, we develop in this paper a nine node shell element based on a new and more efficient mixed formulation. This new formulation is also based on the Hellinger-Reissner principle with independent strain field. However by dividing the assumed strain into a lower order part and a higher order part, it is possible to make the new formulation much more efficient than the conventional mixed formulation. It should be noted that in reference 17 a preliminary study on the effectiveness of the new formulation has been made for plane stress problem. In this reference, it was demonstrated that, for the nine node plane stress element, the new formulation requires less than half of the computing time needed for the conventional mixed formulation to generate an element stiffness matrix. In order to more clearly demonstrate the effectiveness of the new formulation in comparison with the conventional mixed formulation, we will present both formulations. The performance of the new nine node shell element will be tested by solving simple example problems involving very thin plates and shells.

GEOMETRY AND KINEMATICS

Figure 1 illustrates a portion of a curved shell before and after deformation. For convenience, a local orthogonal coordinates system is defined at a point on the shell midsurface in addition to the global coordinates X, Y and Z. Three axes x, y and z of the local coordinate system are parallel to local orthogonal unit vectors $\underset{\sim}{a}_1$, $\underset{\sim}{a}_2$ and $\underset{\sim}{a}_3$ respectively. The unit vectors $\underset{\sim}{a}_1$ and $\underset{\sim}{a}_2$ are tangential to the shell midsurface while $\underset{\sim}{a}_3$ is normal to the surface.

With these coordinate systems, the position vector $\underset{\sim}{X}$ of a generic material point P in the undeformed configuration can be expressed as

$$\underset{\sim}{X} = \underset{\sim}{X}_0 + z\,\underset{\sim}{a}_3 = \underset{\sim}{X}_0 + \zeta\,\frac{t}{2}\,\underset{\sim}{a}_3 \tag{1}$$

where $\underset{\sim}{X}_0$ is the global position vector of point O on the shell midsurface, t is the shell thickness and the nondimensional coordinate ζ runs from -1 to 1. Note that the line connecting point O to point P is normal to the shell midsurface. On the other hand, under the shell assumption, the displacement vector $\underset{\sim}{U}$ of point P with respect to the global coordinate system can be expressed as

$$\underset{\sim}{U} = \underset{\sim}{U}_0 + \zeta\,\frac{t}{2}\,(\underset{\sim}{a}_3' - \underset{\sim}{a}_3) \tag{2}$$

where $\underset{\sim}{U}_0$ is the displacement vector of point O in the global coordinate system and $\underset{\sim}{a}_3'$ is the $\underset{\sim}{a}_3$ vector in the deformed configuration. For small rotation of $\underset{\sim}{a}_3$,

$$\underset{\sim}{a}_3' - \underset{\sim}{a}_3 = \theta_1\,\underset{\sim}{a}_1 + \theta_2\,\underset{\sim}{a}_2 \tag{3}$$

where rotational angles θ_1 and θ_2 are defined around the local y axis and x axis as shown in Fig. 2. If $\underset{\sim}{u}$ represents the displacement vector of point O on the midsurface with components u, v, w in the local coordinate system, the global displacement vector $\underset{\sim}{U}$ can be expressed as follows:

$$\underset{\sim}{U} = \underset{\sim}{T}\,\underset{\sim}{u} + \zeta\,\underset{\sim}{b}\,\underset{\sim}{\theta} \tag{4}$$

where

$$\underset{\sim}{T} = [\underset{\sim}{a}_1\ \underset{\sim}{a}_2\ \underset{\sim}{a}_3] \tag{4a}$$

is the 3 x 3 transformation matrix relating $\underset{\sim}{U}_o$ to $\underset{\sim}{u}$,

$$\underset{\sim}{b} = \frac{t}{2}[\underset{\sim}{a}_1\ \underset{\sim}{a}_2] \tag{4b}$$

and

$$\underset{\sim}{\theta}^T = \lfloor \theta_1\ \theta_2 \rfloor \tag{4c}$$

For a nine node degenerate solid shell element as shown in Fig. 2, the position vector $\underset{\sim}{X}$ of a point in the element can be interpolated from the nodal values using nine-node Lagrange shape functions $N_i(\xi,\eta)$ such that

$$\underset{\sim}{X} = \sum_{i=1}^{9} N_i \underset{\sim}{X}_o^i + \frac{\zeta}{2} \sum_{i=1}^{9} N_i t_i \underset{\sim}{a}_3^i \tag{5}$$

where $\underset{\sim}{X}_o^i$, t_i and $\underset{\sim}{a}_3^i$ are values of $\underset{\sim}{X}_o$, t and $\underset{\sim}{a}_3$ at node i respectively, and ξ and η are parent coordinates. Similarly, the global displacement vector $\underset{\sim}{U}$ is assumed as

$$\underset{\sim}{U} = \sum_{i=1}^{9} N_i \underset{\sim}{T}_i \underset{\sim}{u}_i + \zeta \sum_{i=1}^{9} N_i \underset{\sim}{b}_i \underset{\sim}{\theta}_i \tag{6}$$

where $\underset{\sim}{u}_i$ and $\underset{\sim}{\theta}_i$ are the nodal displacement and rotation vectors respectively.

With the description of geometry and displacement given above it is easy to establish a relationship between the strain vector $\underset{\sim}{E}^G$ in the global coordinate system and the element nodal degrees of freedom vector $\underset{\sim}{q}_e$. Neglecting higher order terms in ζ, $\underset{\sim}{E}^G$ can be written symbolically as

$$\underset{\sim}{E}^G = \underset{\sim}{B}_o^G\,\underset{\sim}{q}_e + \zeta \underset{\sim}{B}_\zeta^G\,\underset{\sim}{q}_e \tag{7}$$

where $\underset{\sim}{B}_o^G$, $\underset{\sim}{B}_\zeta^G$ are matrices relating $\underset{\sim}{E}^G$ to $\underset{\sim}{q}_e$. Subsequently, the strain vector $\underset{\sim}{E}$ defined with respect to the local coordinate system is obtained by transforming the global strain vector in Eq. (7) as follows:

$$\underset{\sim}{E} = \underset{\sim}{T}_E\,\underset{\sim}{E}^G \tag{8}$$

where $\underset{\sim}{T}_E$ is the strain transform matrix. Then $\underset{\sim}{\bar{E}}$ can be written symbolically as

$$\underset{\sim}{\bar{E}} = \begin{Bmatrix} \underset{\sim}{\bar{\varepsilon}} \\ \underset{\sim}{\bar{\gamma}} \end{Bmatrix} + \zeta \begin{Bmatrix} \underset{\sim}{\bar{\kappa}} \\ \underset{\sim}{0} \end{Bmatrix} \tag{9}$$

where

$$\underset{\sim}{\bar{\varepsilon}} = \begin{Bmatrix} \bar{\varepsilon}_{xx} \\ \bar{\varepsilon}_{yy} \\ \bar{\varepsilon}_{xy} \end{Bmatrix} = \underset{\sim}{B}_e \underset{\sim}{q}_e = \text{inplane strain vector} \tag{9a}$$

$$\zeta\underset{\sim}{\bar{\kappa}} = \zeta \begin{Bmatrix} \bar{\kappa}_{xx} \\ \bar{\kappa}_{yy} \\ \bar{\kappa}_{xy} \end{Bmatrix} = \zeta \underset{\sim}{B}_\kappa \underset{\sim}{q}_e = \text{bending strain vector} \tag{9b}$$

$$\underset{\sim}{\bar{\gamma}} = \begin{Bmatrix} \bar{\varepsilon}_{yz} \\ \bar{\varepsilon}_{zx} \end{Bmatrix} = \underset{\sim}{B}_\gamma \underset{\sim}{q}_e = \text{transverse shear strain vector} \tag{9c}$$

In the above expression $\underset{\sim}{B}_e$, $\underset{\sim}{B}_\kappa$ and $\underset{\sim}{B}_\gamma$ are matrices dependent only on ξ and η coordinates. A similar expression holds for the virtual strain vectors $\delta\underset{\sim}{\bar{\varepsilon}}$, $\zeta\delta\underset{\sim}{\bar{\kappa}}$ and $\delta\underset{\sim}{\bar{\gamma}}$.

MIXED FORMULATION FOR SHELL ELEMENTS

The functional π_R for the Hellinger-Reissner principle is expressed as follows:

$$\pi_R = \sum \int_{V_e} (\underset{\sim}{E}^T \underset{\sim}{C} \underset{\sim}{\bar{E}} - \frac{1}{2} \underset{\sim}{E}^T \underset{\sim}{C} \underset{\sim}{E}) dV_e - W_o \tag{10}$$

where, for shells,

$$\underset{\sim}{E}^T = \lfloor E_{xx} \; E_{yy} \; E_{xy} \; E_{yz} \; E_{zx} \rfloor$$

= independent local strain vector

$$\underset{\sim}{\bar{E}}^T = \lfloor \bar{E}_{xx} \; \bar{E}_{yy} \; \bar{E}_{xy} \; \bar{E}_{yz} \; \bar{E}_{zx} \rfloor$$

= local strain vector derived from displacement field

W_o = applied load term

V_e = volume of element

$$\underset{\sim}{C} = \begin{bmatrix} \underset{\sim}{C}_1 & \underset{\sim}{0} \\ \underset{\sim}{0} & \underset{\sim}{C}_2 \end{bmatrix} = 5\text{x}5 \text{ elastic coefficient matrix}$$

$\underset{\sim}{C}_1$ = 3x3 matrix

$\underset{\sim}{C}_2$ = 2x2 matrix

The summation sign indicates summation or assembly over all elements.

In accordance with Eq. (9), the independent local strain vector $\underset{\sim}{E}$ can be separated into inplane, bending and transverse shear strains such that

$$\underset{\sim}{E} = \begin{Bmatrix} \underset{\sim}{\varepsilon} \\ \underset{\sim}{\gamma} \end{Bmatrix} + \zeta \begin{Bmatrix} \underset{\sim}{\kappa} \\ \underset{\sim}{0} \end{Bmatrix} \tag{11}$$

where

$$\underset{\sim}{\varepsilon} = \begin{Bmatrix} \varepsilon_{xx} \\ \varepsilon_{yy} \\ \varepsilon_{xy} \end{Bmatrix} = \text{independent inplane strain vector} \tag{11a}$$

$$\zeta\underset{\sim}{\kappa} = \zeta \begin{Bmatrix} \kappa_{xx} \\ \kappa_{yy} \\ \kappa_{xy} \end{Bmatrix} = \text{independent bending strain vector} \tag{11b}$$

and

$$\underset{\sim}{\gamma} = \begin{Bmatrix} \varepsilon_{yz} \\ \varepsilon_{zx} \end{Bmatrix} = \text{indenpendent transverse shear strain vector.} \tag{11c}$$

Moreover, in anticipation of applying a finite element approximation, we may write dV_e as

$$dV_e = \left| \underset{\sim}{J} \right| d\xi \, d\eta \, d\zeta \tag{12a}$$

where $\left| \underset{\sim}{J} \right|$ is the determinant of the three dimensional Jacobian matrix $\underset{\sim}{J}$.

However $|\underset{\sim}{J}|$ changes very little along the shell thickness and thus it is possible to assume

$$dV_e = |\underset{\sim}{J}|_{\zeta=0} \, d\xi \, dn \, d\zeta \tag{12b}$$

Substituting Eqs. (9) and (11) into Eq. (10) and integrating in the ζ direction, the functional π_R becomes

$$\begin{aligned}\pi_R = \sum \Big[& \int (\underset{\sim}{\varepsilon}^T \underset{\sim}{C}_e \, \bar{\underset{\sim}{\varepsilon}} - \tfrac{1}{2} \underset{\sim}{\varepsilon}^T \underset{\sim}{C}_e \, \underset{\sim}{\varepsilon}) \, dA \\ & + \int (\underset{\sim}{\kappa}^T \underset{\sim}{C}_\kappa \, \bar{\underset{\sim}{\kappa}} - \tfrac{1}{2} \underset{\sim}{\kappa}^T \underset{\sim}{C}_\kappa \, \underset{\sim}{\kappa}) \, dA \\ & + \int (\underset{\sim}{\chi}^T \underset{\sim}{C}_\gamma \, \bar{\underset{\sim}{\chi}} - \tfrac{1}{2} \underset{\sim}{\chi}^T \underset{\sim}{C}_\gamma \, \underset{\sim}{\chi}) \, dA \Big] - W_o \end{aligned} \tag{13}$$

where

$$\underset{\sim}{C}_e = \int_{-1}^{1} \underset{\sim}{C}_1 \, d\zeta \tag{13a}$$

$$\underset{\sim}{C}_\kappa = \int_{-1}^{1} \zeta^2 \, \underset{\sim}{C}_1 \, d\zeta \tag{13b}$$

$$\underset{\sim}{C}_\gamma = \int_{-1}^{1} \underset{\sim}{C}_2 \, d\zeta \tag{13c}$$

$$dA = |\underset{\sim}{J}|_{\zeta=0} \, d\xi \, dn \tag{13d}$$

The strain vectors $\bar{\underset{\sim}{\varepsilon}}$, $\zeta\bar{\underset{\sim}{\kappa}}$ and $\bar{\underset{\sim}{\chi}}$ obtained from the assumed displacement field are given in Eqs. (9a) to (9c).

(a) Conventional Formulation

In the conventional mixed formulation, independent inplane strain, bending strain and transverse shear strain are assumed to have polynomial distributions in terms of parent coordinates ξ and η. Symbolically,

$$\underset{\sim}{\varepsilon} = \underset{\sim}{P}_e \, (\xi,\eta) \, \underset{\sim}{\alpha} \tag{14a}$$

$$\underset{\sim}{\kappa} = \underset{\sim}{P}_\kappa \, (\xi,\eta) \, \underset{\sim}{\beta}_\kappa \tag{14b}$$

$$\underset{\sim}{\chi} = \underset{\sim}{P}_\gamma \, (\xi,\eta) \, \underset{\sim}{\beta} \tag{14c}$$

where $\underset{\sim}{P}_e$, $\underset{\sim}{P}_\kappa$, $\underset{\sim}{P}_\gamma$ are the shape function matrices of assumed strain fields and $\underset{\sim}{\alpha}$, $\underset{\sim}{\beta}_\kappa$, $\underset{\sim}{\beta}$ are the assumed strain parameters chosen independently for each element.

Substituting Eq. (9a) to Eq. (9c) and Eq. (14a) to (14c) into the functional π_R,

$$\pi_R = \sum[(\underset{\sim}{\alpha}^T \underset{\sim}{G}_e g_e - \frac{1}{2}\underset{\sim}{\alpha}^T \underset{\sim}{H}_e \underset{\sim}{\alpha}) + (\underset{\sim}{\beta}_\kappa^T \underset{\sim}{G}_\kappa g_e - \frac{1}{2}\underset{\sim}{\beta}_\kappa^T \underset{\sim}{H}_\kappa \underset{\sim}{\beta}_\kappa)$$

$$+ (\underset{\sim}{\beta}^T \underset{\sim}{G}_\gamma g_e - \frac{1}{2}\underset{\sim}{\beta}^T \underset{\sim}{H}_\gamma \underset{\sim}{\beta})] - W_o \tag{15}$$

where

$$\underset{\sim}{G}_e = \int \underset{\sim}{P}_e^T \underset{\sim}{C}_e \underset{\sim}{B}_e \, dA \tag{15a}$$

$$\underset{\sim}{H}_e = \int \underset{\sim}{P}_e^T \underset{\sim}{C}_e \underset{\sim}{P}_e \, dA \tag{15b}$$

$$\underset{\sim}{G}_\kappa = \int \underset{\sim}{P}_\kappa^T \underset{\sim}{C}_\kappa \underset{\sim}{B}_\kappa \, dA \tag{15c}$$

$$\underset{\sim}{H}_\kappa = \int \underset{\sim}{P}_\kappa^T \underset{\sim}{C}_\kappa \underset{\sim}{P}_\kappa \, dA \tag{15d}$$

$$\underset{\sim}{G}_\gamma = \int \underset{\sim}{P}_\gamma^T \underset{\sim}{C}_\gamma \underset{\sim}{B}_\gamma \, dA \tag{15e}$$

$$\underset{\sim}{H}_\gamma = \int \underset{\sim}{P}_\gamma^T \underset{\sim}{C}_\gamma \underset{\sim}{P}_\gamma dA \tag{15f}$$

Setting $\delta\pi_R = 0$ with respect to $\underset{\sim}{\alpha}$, $\underset{\sim}{\beta}_\kappa$ and $\underset{\sim}{\beta}$ respectively,

$$\underset{\sim}{G}_e \, g_e - \underset{\sim}{H}_e \, \underset{\sim}{\alpha} = 0 \tag{16a}$$

$$\underset{\sim}{G}_\kappa \, g_e - \underset{\sim}{H}_\kappa \, \underset{\sim}{\beta}_\kappa = 0 \tag{16b}$$

$$\underset{\sim}{G}_\gamma \, g_e - \underset{\sim}{H}_\gamma \, \underset{\sim}{\beta} = 0 \tag{16c}$$

These three equations represent compatibility in discretized form. Solving these equations, strain parameter vectors $\underset{\sim}{\alpha}$, $\underset{\sim}{\beta}_\kappa$ and $\underset{\sim}{\beta}$ are expressed in terms of element nodal degrees of freedom vector g_e as follows:

$$\underset{\sim}{\alpha} = \underset{\sim}{H}_e^{-1} \, \underset{\sim}{G}_e \, g_e \tag{17a}$$

$$\underset{\sim}{\beta}_\kappa = \underset{\sim}{H}_\kappa^{-1} \, \underset{\sim}{G}_\kappa \, g_e \tag{17b}$$

$$\underset{\sim}{\beta} = \underset{\sim}{H}_\gamma^{-1} \, \underset{\sim}{G}_\gamma \, g_e \tag{17c}$$

Introducing $\underset{\sim}{\alpha}$, $\underset{\sim}{\beta}_\kappa$ and $\underset{\sim}{\beta}$ into Eq. (15), the Hellinger-Reissner functional can be written as

$$\pi_R = \sum (\frac{1}{2} \underset{\sim}{q}_e^T \underset{\sim}{K}_e \underset{\sim}{q}_e - \underset{\sim}{q}_e^T \underset{\sim}{Q}_e) \tag{18}$$

where

$$\underset{\sim}{K}_e = \underset{\sim}{G}_e^T \underset{\sim}{H}_e^{-1} \underset{\sim}{G}_e + \underset{\sim}{G}_\kappa^T \underset{\sim}{H}_\kappa^{-1} \underset{\sim}{G}_\kappa + \underset{\sim}{G}_\gamma^T \underset{\sim}{H}_\gamma^{-1} \underset{\sim}{G}_\gamma \tag{18a}$$

is the element stiffness matrix and

$$\sum \underset{\sim}{q}_e^T \underset{\sim}{Q}_e = W_o \tag{18b}$$

with $\underset{\sim}{Q}_e$ as the element load vector.

Since bending strain is irrelevant to locking, we may utilize, for the finite element approximation, a modified Hellinger-Reissner principle which is obtained by setting $\underset{\sim}{\kappa} = \overline{\underset{\sim}{\kappa}}$ in Eq. (13). A finite element formulation based on this modified Hellinger-Reissner principle was developed in reference 15. For the purpose of identification, the formulation based on this modified Hellinger-Reissner principle is called conventional formulation II while the formulation described in this section is called conventional formulation I.

(b) New Formulation

The proposed new formulation is also based on the Hellinger-Reissner principle with the functional given in Eq. (13). However, as suggested in reference 17, in the new formulation the independent assumed strains are written as

$$\underset{\sim}{\varepsilon} = \underset{\sim}{\varepsilon}_L + \underset{\sim}{\varepsilon}_H \tag{19a}$$

$$\underset{\sim}{\kappa} = \underset{\sim}{\kappa}_L + \underset{\sim}{\kappa}_H \tag{19b}$$

$$\underset{\sim}{\gamma} = \underset{\sim}{\gamma}_L + \underset{\sim}{\gamma}_H \tag{19c}$$

where $\underset{\sim}{\varepsilon}_L$, $\underset{\sim}{\kappa}_L$ and $\underset{\sim}{\gamma}_L$ are the independent strain vectors with lower order assumed

polynomial terms in ξ and η. On the other hand, $\underset{\sim}{\varepsilon}_H$, $\underset{\sim}{\kappa}_H$ and $\underset{\sim}{\chi}_H$ are the higher order strain vectors which contain higher order terms in ξ and η. More discussion on these strain vectors will be given later. Inserting Eqs. (19a-c) into Eq. (13), the functional π_R becomes

$$\pi_R = U_I + U_B + U_S - W_o \tag{20}$$

where

$$U_I = \sum \left[\int (\underset{\sim}{\varepsilon}_L^T \underset{\sim}{C}_e \bar{\underset{\sim}{\varepsilon}} - \frac{1}{2} \underset{\sim}{\varepsilon}_L^T \underset{\sim}{C}_e \underset{\sim}{\varepsilon}_L) dA + \int \underset{\sim}{\varepsilon}_H^T \underset{\sim}{C}_e \bar{\underset{\sim}{\varepsilon}} dA \right.$$

$$\left. - \int \underset{\sim}{\varepsilon}_H^T \underset{\sim}{C}_e \underset{\sim}{\varepsilon}_L dA - \frac{1}{2} \int \underset{\sim}{\varepsilon}_H^T \underset{\sim}{C}_e \underset{\sim}{\varepsilon}_H dA \right] \tag{20a}$$

$$U_B = \sum \left[\int (\underset{\sim}{\kappa}_L^T \underset{\sim}{C}_\kappa \bar{\underset{\sim}{\kappa}} - \frac{1}{2} \underset{\sim}{\kappa}_L^T \underset{\sim}{C}_\kappa \underset{\sim}{\kappa}_L) dA + \int \underset{\sim}{\kappa}_H^T \underset{\sim}{C}_\kappa \bar{\underset{\sim}{\kappa}} dA \right.$$

$$\left. - \int \underset{\sim}{\kappa}_H^T \underset{\sim}{C}_\kappa \underset{\sim}{\kappa}_L dA - \frac{1}{2} \int \underset{\sim}{\kappa}_H^T \underset{\sim}{C}_\kappa \underset{\sim}{\kappa}_H dA \right] \tag{20b}$$

and

$$U_S = \sum \left[\int (\underset{\sim}{\chi}_L^T \underset{\sim}{C}_\gamma \bar{\underset{\sim}{\chi}} - \frac{1}{2} \underset{\sim}{\chi}_L^T \underset{\sim}{C}_\gamma \underset{\sim}{\chi}_L) dA + \int \underset{\sim}{\chi}_H^T \underset{\sim}{C}_\gamma \bar{\underset{\sim}{\chi}} dA \right.$$

$$\left. - \int \underset{\sim}{\chi}_H^T \underset{\sim}{C}_\gamma \underset{\sim}{\chi}_L dA - \frac{1}{2} \int \underset{\sim}{\chi}_H^T \underset{\sim}{C}_\gamma \underset{\sim}{\chi}_H dA \right] \tag{20c}$$

For the numerical integration of terms in Eqs. (20a-c), we may use a lower order integration rule for the terms which contain lower order assumed strains $\underset{\sim}{\varepsilon}_L$, $\underset{\sim}{\kappa}_L$ and $\underset{\sim}{\chi}_L$ respectively. For the remaining terms a higher order integraion rule is used. Then the lower order independent strains may be assumed in terms of displacement-dependent strains $\bar{\underset{\sim}{\varepsilon}}$, $\bar{\underset{\sim}{\kappa}}$ and $\bar{\underset{\sim}{\chi}}$ evaluated at the lower order integration points as follows:

$$\underset{\sim}{\varepsilon}_L = \sum_{i=1}^{N_L} \tilde{N}_i(\xi,\eta) \bar{\underset{\sim}{\varepsilon}}_i \tag{21a}$$

$$\underset{\sim}{\kappa}_L = \sum_{i=1}^{N_L} \tilde{N}_i(\xi,\eta)\overline{\underset{\sim}{\kappa}}_i \tag{21b}$$

$$\underset{\sim}{\gamma}_L = \sum_{i=1}^{N_L} \tilde{N}_i(\xi,\eta)\overline{\underset{\sim}{\gamma}}_i \tag{21c}$$

where $\tilde{N}_i$ is the shape function such that $\tilde{N}_i = 1$ at the point i of the lower order integration points and zero at other points, $\overline{\underset{\sim}{\varepsilon}}_i$, $\overline{\underset{\sim}{\kappa}}_i$ and $\overline{\underset{\sim}{\gamma}}_i$ are evaluated at integration point i, and N_L is the number of the lower order integration points. In another word, we can set

$$\underset{\sim}{\varepsilon}_L = \overline{\underset{\sim}{\varepsilon}} \tag{22a}$$

$$\underset{\sim}{\kappa}_L = \overline{\underset{\sim}{\kappa}} \tag{22b}$$

$$\underset{\sim}{\gamma}_L = \overline{\underset{\sim}{\gamma}} \tag{22c}$$

at the lower order integration points.

Introducing Eqs. (22a-c) into Eqs. (20a-c) respectively,

$$U_I = \sum \left[\frac{1}{2}\int_L \underset{\sim}{\varepsilon}_L^T \underset{\sim}{C}_e \underset{\sim}{\varepsilon}_L \, dA + \int_H \underset{\sim}{\varepsilon}_H^T \underset{\sim}{C}_e \overline{\underset{\sim}{\varepsilon}} \, dA - \int_L \underset{\sim}{\varepsilon}_H^T \underset{\sim}{C}_e \underset{\sim}{\varepsilon}_L \, dA - \frac{1}{2}\int_H \underset{\sim}{\varepsilon}_H^T \underset{\sim}{C}_e \underset{\sim}{\varepsilon}_H \, dA\right] \tag{23a}$$

$$U_B = \sum \left[\frac{1}{2}\int_L \underset{\sim}{\kappa}_L^T \underset{\sim}{C}_\kappa \underset{\sim}{\kappa}_L \, dA + \int_H \underset{\sim}{\kappa}_H^T \underset{\sim}{C}_\kappa \overline{\underset{\sim}{\kappa}} \, dA - \int_L \underset{\sim}{\kappa}_H^T \underset{\sim}{C}_\kappa \underset{\sim}{\kappa}_L \, dA - \frac{1}{2}\int_H \underset{\sim}{\kappa}_H^T \underset{\sim}{C}_\kappa \underset{\sim}{\kappa}_H \, dA\right] \tag{23b}$$

$$U_S = \sum \left[\frac{1}{2}\int_L \underset{\sim}{\gamma}_L^T \underset{\sim}{C}_\gamma \underset{\sim}{\gamma}_L \, dA + \int_H \underset{\sim}{\gamma}_H^T \underset{\sim}{C}_\gamma \overline{\underset{\sim}{\gamma}} dA - \int_L \underset{\sim}{\gamma}_H^T \underset{\sim}{C}_\gamma \underset{\sim}{\gamma}_L \, dA - \frac{1}{2}\int_H \underset{\sim}{\gamma}_H^T \underset{\sim}{C}_\gamma \underset{\sim}{\gamma}_H \, dA\right] \tag{23c}$$

In Eqs. (23a-c), letters L and H under the integral signs indicate the lower

order integration and the higher order integration rules respectively.

The higher order strains are assumed to have higher order terms of ξ and η such that

$$\underset{\sim}{\varepsilon}_H = \overline{\underset{\sim}{P}}_e \ (\xi,\eta) \ \underset{\sim}{\alpha} \tag{24a}$$

$$\underset{\sim}{\kappa}_H = \overline{\underset{\sim}{P}}_\kappa \ (\xi,\eta) \ \underset{\sim}{\beta}_\kappa \tag{24b}$$

$$\underset{\sim}{\gamma}_H = \overline{\underset{\sim}{P}}_\gamma \ (\xi,\eta) \ \underset{\sim}{\beta} \tag{24c}$$

where $\overline{\underset{\sim}{P}}_e$, $\overline{\underset{\sim}{P}}_\kappa$ and $\overline{\underset{\sim}{P}}_\gamma$ are the shape function matrices of the higher order assumed strains and $\underset{\sim}{\alpha}$, $\underset{\sim}{\beta}_\kappa$ and $\underset{\sim}{\beta}$ are the associated strain parameters.

Noting that $\underset{\sim}{\varepsilon}_L = \underset{\sim}{\varepsilon}$, $\underset{\sim}{\kappa}_L = \overline{\underset{\sim}{\kappa}}$ and $\gamma_L = \overline{\gamma}$ at lower order integration points, and introducing Eqs. (9a-c) and (24a-c) into Eqs. (23a) to (23c) we obtain the following expressions:

$$U_I = \sum \left(\frac{1}{2} q_e^T \underset{\sim}{K}_{I_L} q_e + \underset{\sim}{\alpha}^T \overline{\underset{\sim}{G}}_e q_e - \frac{1}{2} \underset{\sim}{\alpha}^T \overline{\underset{\sim}{H}}_e \underset{\sim}{\alpha}\right) \tag{25}$$

where

$$\underset{\sim}{K}_{I_L} = \int_L \underset{\sim}{B}_e^T \underset{\sim}{C}_e \underset{\sim}{B}_e \, dA \tag{25a}$$

$$\overline{\underset{\sim}{G}}_e = \int_H \overline{\underset{\sim}{P}}_e^T \underset{\sim}{C}_e \underset{\sim}{B}_e \, dA - \int_L \overline{\underset{\sim}{P}}_e^T \underset{\sim}{C}_e \underset{\sim}{B}_e \, dA \tag{25b}$$

$$\overline{\underset{\sim}{H}}_e = \int_H \overline{\underset{\sim}{P}}_e^T \underset{\sim}{C}_e \overline{\underset{\sim}{P}}_e \, dA \tag{25c}$$

and $$U_B = \sum \left(\frac{1}{2} q_e^T \underset{\sim}{K}_{B_L} q_e + \underset{\sim}{\beta}_\kappa^T \overline{\underset{\sim}{G}}_\kappa q_e - \frac{1}{2} \underset{\sim}{\beta}_\kappa^T \overline{\underset{\sim}{H}}_\kappa \underset{\sim}{\beta}_\kappa\right) \tag{26}$$

where $$\underset{\sim}{K}_{B_L} = \int_L \underset{\sim}{B}_\kappa^T \underset{\sim}{C}_\kappa \underset{\sim}{B}_\kappa \, dA \tag{26a}$$

$$\overline{\underset{\sim}{G}}_\kappa = \int_H \overline{\underset{\sim}{P}}_\kappa^T \underset{\sim}{C}_\kappa \underset{\sim}{B}_\kappa \, dA - \int \overline{\underset{\sim}{P}}_\kappa^T \underset{\sim}{C}_\kappa \underset{\sim}{B}_\kappa \, dA \tag{26b}$$

$$\overline{\underset{\sim}{H}}_\kappa = \int_H \overline{\underset{\sim}{P}}_\kappa^T \underset{\sim}{C}_\kappa \overline{\underset{\sim}{P}}_\kappa \, dA \tag{26c}$$

and $$U_S = \sum \left(\frac{1}{2} g_e^T \underset{\sim}{K}_{S_L} g_e + \underset{\sim}{\beta}^T \overline{\underset{\sim}{G}}_\gamma g_e - \frac{1}{2} \underset{\sim}{\beta}^T \overline{\underset{\sim}{H}}_\gamma \underset{\sim}{\beta}\right) \tag{27}$$

where $$\underset{\sim}{K}_{S_L} = \int_L \underset{\sim}{B}_\gamma^T \underset{\sim}{C}_\gamma \underset{\sim}{B}_\gamma \, dA \tag{27a}$$

$$\overline{\underset{\sim}{G}}_\gamma = \int_H \overline{\underset{\sim}{P}}_\gamma^T \underset{\sim}{C}_\gamma \underset{\sim}{B}_\gamma \, dA - \int_L \overline{\underset{\sim}{P}}_\gamma^T \underset{\sim}{C}_\gamma \underset{\sim}{B}_\gamma \, dA \tag{27b}$$

$$\overline{\underset{\sim}{H}}_\gamma = \int_H \overline{\underset{\sim}{P}}_\gamma^T \underset{\sim}{C}_\gamma \overline{\underset{\sim}{P}}_\gamma \, dA \tag{27c}$$

Substituting Eqs. (25), (26) and (27) into Eq. (20), the functional π_R can be expressed as

$$\begin{aligned}\pi_R = \sum \Big[&\frac{1}{2} g_e^T \underset{\sim}{K}_{I_L} g_e + \underset{\sim}{\alpha}^T \overline{\underset{\sim}{G}}_e g_e - \frac{1}{2} \underset{\sim}{\alpha}^T \overline{\underset{\sim}{H}}_e \underset{\sim}{\alpha} \\ &+ \frac{1}{2} g_e^T \underset{\sim}{K}_{B_L} g_e + \underset{\sim}{\beta}_\kappa^T \overline{\underset{\sim}{G}}_\kappa g_e - \frac{1}{2} \underset{\sim}{\beta}_\kappa^T \overline{\underset{\sim}{H}}_\kappa \underset{\sim}{\beta}_\kappa \\ &+ \frac{1}{2} g_e^T \underset{\sim}{K}_{S_L} g_e + \underset{\sim}{\beta}^T \overline{\underset{\sim}{G}}_\gamma g_e - \frac{1}{2} \underset{\sim}{\beta}^T \overline{\underset{\sim}{H}}_\gamma \underset{\sim}{\beta} \\ &- g_e^T \underset{\sim}{Q}_e\Big]\end{aligned} \tag{28}$$

Taking $\delta\pi_R = 0$ with respect to $\underset{\sim}{\alpha}$, $\underset{\sim}{\beta}_\kappa$ and $\underset{\sim}{\beta}$ results in three compatibility relations in discretized form similar to Eqs. (16a-c). Solving them,

$$\underset{\sim}{\alpha} = \overline{\underset{\sim}{H}}_e^{-1} \overline{\underset{\sim}{G}}_e g_e \tag{29a}$$

$$\underset{\sim}{\beta}_\kappa = \overline{\underset{\sim}{H}}_K^{-1} \overline{\underset{\sim}{G}}_K g_e \tag{29b}$$

$$\underset{\sim}{\beta} = \overline{\underset{\sim}{H}}_\gamma^{-1} \overline{\underset{\sim}{G}}_\gamma g_e \tag{29c}$$

Substituting these equations into Eq. (28) leads to

$$\pi_R = \sum \left(\frac{1}{2} g_e^T \underset{\sim}{K}_e g_e - g_e^T \underset{\sim}{Q}_e\right) \tag{30}$$

where the element stiffness matrix $\underset{\sim}{K}_e$ is written as

$$\underset{\sim}{K}_e = \underset{\sim}{K}_L + \underset{\sim}{K}_S \tag{31}$$

with

$$\underset{\sim}{K}_L = \underset{\sim}{K}I_L + \underset{\sim}{K}B_L + \underset{\sim}{K}S_L \tag{31a}$$

and

$$\underset{\sim}{K}_S = \overline{\underset{\sim}{G}}_e^T \overline{\underset{\sim}{H}}_e^{-1} \overline{\underset{\sim}{G}}_e + \overline{\underset{\sim}{G}}_\kappa^T \overline{\underset{\sim}{H}}_\kappa^{-1} \overline{\underset{\sim}{G}}_\kappa + \overline{\underset{\sim}{G}}_\gamma^T \overline{\underset{\sim}{H}}_\gamma^{-1} \overline{\underset{\sim}{G}}_\gamma \tag{31b}$$

It should be noted that the size of $\overline{\underset{\sim}{G}}_e$, $\overline{\underset{\sim}{G}}_\kappa$, $\overline{\underset{\sim}{G}}_\gamma$, $\overline{\underset{\sim}{H}}_e$, $\overline{\underset{\sim}{H}}_\kappa$ and $\overline{\underset{\sim}{H}}_\gamma$ matrices in the new formulation are much smaller than $\underset{\sim}{G}_e$, $\underset{\sim}{G}_\kappa$, $\underset{\sim}{G}_\gamma$, $\underset{\sim}{H}_e$, $\underset{\sim}{H}_\kappa$ and $\underset{\sim}{H}_\gamma$ in the conventional formulation. In addition, in order to compute $\overline{\underset{\sim}{G}}_e$, $\overline{\underset{\sim}{G}}_\kappa$, $\overline{\underset{\sim}{G}}_\gamma$ and $\underset{\sim}{K}_L$ in Eqs. (31a,b), it is necessary to evaluate B_e, B_κ, B_γ matrices and $|\underset{\sim}{J}|$ at the lower order integration points. To save computing time their values are interpolated from the values of $\underset{\sim}{B}_e$, $\underset{\sim}{B}_\kappa$, $\underset{\sim}{B}_\gamma$ and $|\underset{\sim}{J}|$ evaluated at the higher order integration points as follows:

$$\underset{\sim}{B}_e = \sum_{i=1}^{N_H} \overline{N}_i\ (\xi,\eta)\ \underset{\sim}{B}_e^i \tag{32a}$$

$$\underset{\sim}{B}_\kappa = \sum_{i=1}^{N_H} \overline{N}_i\ (\xi,\eta)\ \underset{\sim}{B}_\kappa^i \tag{32b}$$

$$\underset{\sim}{B}_\gamma = \sum_{i=1}^{N_H} \overline{N}_i\ (\xi,\eta)\ \underset{\sim}{B}_\gamma^i \tag{32c}$$

$$|\underset{\sim}{J}| = \sum_{i=1}^{N_H} \overline{N}_i\ (\xi,\eta)\ |\underset{\sim}{J}|^i \tag{32d}$$

where $\underset{\sim}{B}_e^i$, $\underset{\sim}{B}_\kappa^i$, $\underset{\sim}{B}_\gamma^i$ and $|\underset{\sim}{J}|^i$ are evaluated at the higher order integration point i, and $\overline{N}_i$ is the shape function such that $\overline{N}_i = 1$ at higher order integration point i and zero at the other integration points and N_H is the number of the higher order integration points.

After assembling element stiffness matrices and load vectors and solving for the nodal displacement vector, the strain vectors are determined as

follows:

$$\underset{\sim}{\varepsilon} = \underset{\sim}{\varepsilon}_L + \overline{\underset{\sim}{P}}_e \overline{\underset{\sim}{H}}_e^{-1} \overline{\underset{\sim}{G}}_e \underset{\sim}{q}_e \tag{33a}$$

$$\underset{\sim}{\kappa} = \underset{\sim}{\kappa}_L + \overline{\underset{\sim}{P}}_\kappa \overline{\underset{\sim}{H}}_\kappa^{-1} \overline{\underset{\sim}{G}}_\kappa \underset{\sim}{q}_e \tag{33b}$$

$$\underset{\sim}{\gamma} = \underset{\sim}{\gamma}_L + \overline{\underset{\sim}{P}}_\gamma \overline{\underset{\sim}{H}}_\gamma^{-1} \overline{\underset{\sim}{G}}_\gamma \underset{\sim}{q}_e \tag{33c}$$

Then stress $\underset{\sim}{\sigma}$ is determined from Eqs. (33a-c) and the stress-strain relation.

NINE NODE SHELL ELEMENT

The key to a successful application of the mixed formulation is a judicous choice of assumed strain. Especially for the purpose of eliminating locking it is desirable to choose the simplest assumed strain [2]. However an excessively simple form of assumed strain triggers spurious kinematic modes, some of which are commutable or compatible and do not disappear even when elements are assembled. This leads to an unstable global model. Therefore assumed strain must be chosen such that the element is free of both undesirable locking and spurious kinematic modes. This often leads to an element which is not invariant. Invariance is not a critcal issue as long as element characteristics do not change significantly with coordinate systems. However in the present study, we enforce invariance by assigning a particular local coordinate system for a given element geometry as follows:

For the nine node shell element as shown in Fig. 2, the local coordinate system is defined first by determining two unit vectors $\underset{\sim}{v}_1$ and $\underset{\sim}{v}_2$ at $\xi = \eta = \zeta = 0$ point such that

$$\underset{\sim}{v}_1 = \frac{\partial \underset{\sim}{X}_o}{\partial \xi} \Big/ \left| \frac{\partial \underset{\sim}{X}_o}{\partial \xi} \right| \tag{34a}$$

$$\underset{\sim}{v}_2 = \frac{\partial \underset{\sim}{X}_o}{\partial \eta} \Big/ \left| \frac{\partial \underset{\sim}{X}_o}{\partial \eta} \right| \tag{34b}$$

The angle θ_o between these two unit vectors is calculated from the following

equation:

$$\cos\theta_o = \underset{\sim}{v}_1 \cdot \underset{\sim}{v}_2 \tag{35}$$

Then, if θ_o is less than or equal to 90^o, unit vector $\underset{\sim}{a}_1$ in the x direction of local coordinate system is chosen to be parallel with ξ such that

$$\underset{\sim}{a}_1 = \frac{\partial \underset{\sim}{X}_o}{\partial \xi} \Big/ \left| \frac{\partial \underset{\sim}{X}_o}{\partial \xi} \right| \tag{36a}$$

Otherwise $\underset{\sim}{a}_1$ is parallel with η such that

$$\underset{\sim}{a}_1 = \frac{\partial \underset{\sim}{X}_o}{\partial \eta} \Big/ \left| \frac{\partial \underset{\sim}{X}_o}{\partial \eta} \right| \tag{36b}$$

To determine the $\underset{\sim}{a}_3$ vector normal to the shell midsurface, first a unit vector $\underset{\sim}{a}'_2$ is defined as follows:

$$\underset{\sim}{a}'_2 = \frac{\partial \underset{\sim}{X}_o}{\partial \eta} \Big/ \left| \frac{\partial \underset{\sim}{X}_o}{\partial \eta} \right| \quad \text{for } \theta_o \leq 90^o, \tag{37a}$$

$$\underset{\sim}{a}'_2 = \frac{\partial \underset{\sim}{X}_o}{\partial \xi} \Big/ \left| \frac{\partial \underset{\sim}{X}_o}{\partial \xi} \right| \quad \text{for } \theta_o > 90^o. \tag{37b}$$

Then the $\underset{\sim}{a}_3$ vector is obtained by

$$\underset{\sim}{a}_3 = \underset{\sim}{a}_1 \times \underset{\sim}{a}'_2 \Big/ \left| \underset{\sim}{a}_1 \times \underset{\sim}{a}'_2 \right| \tag{38}$$

and the unit vector $\underset{\sim}{a}_2$ in the y direction of local coordinate system is determined as

$$\underset{\sim}{a}_2 = \underset{\sim}{a}_3 \times \underset{\sim}{a}_1 \tag{39}$$

Note that, while $\underset{\sim}{v}_1$ and $\underset{\sim}{v}_2$ are determined at $\xi=\eta=\zeta=0$ point, $\underset{\sim}{a}_1$, $\underset{\sim}{a}_2$ and $\underset{\sim}{a}_3$ can be computed at any point on the shell midsurface. Especially $\underset{\sim}{a}_1$, $\underset{\sim}{a}_2$ and $\underset{\sim}{a}_3$ are needed at integration points to establish a local orthogonal coordinate system. Note that the definition as described here results in a unique local coordinate system for a given element geometry.

For the nine node shell element based on the conventional formulation, we assume the independent strain fields in the local coordinate system as follows:

$$\underset{\sim}{\varepsilon} = \underset{\sim}{P}_e \, \underset{\sim}{\alpha} \tag{40}$$

where

$$\underset{\sim}{P}_e = \begin{bmatrix} 1 & \xi & \eta & \xi\eta & 0 & 0 & 0 & 0 & 0 & 0 & 0 & 0 & f & 0 \\ 0 & 0 & 0 & 0 & 1 & \xi & \eta & \xi\eta & 0 & 0 & 0 & 0 & 0 & g \\ 0 & 0 & 0 & 0 & 0 & 0 & 0 & 0 & 1 & \xi & \eta & \xi\eta & 0 & 0 \end{bmatrix} \tag{40a}$$

$$\underset{\sim}{\alpha}^T = \lfloor \alpha_1, \alpha_2, \ldots\ldots, \alpha_{14} \rfloor \tag{40b}$$

and

$$\underset{\sim}{\kappa} = \underset{\sim}{P}_\kappa \, \underset{\sim}{\beta}_\kappa \tag{41}$$

where

$$\underset{\sim}{P}_\kappa = \underset{\sim}{P}_e \tag{41a}$$

$$\underset{\sim}{\beta}_\kappa = \lfloor \beta_{\kappa 1}, \beta_{\kappa 2}, \ldots\ldots, \beta_{\kappa 14} \rfloor \tag{41b}$$

and

$$\chi = \underset{\sim}{P}_\gamma \, \underset{\sim}{\beta} \tag{42}$$

where

$$\underset{\sim}{P}_\gamma = \begin{bmatrix} 1 & \xi & \eta & \xi\eta & 0 & 0 & 0 & 0 & g & 0 \\ 0 & 0 & 0 & 0 & 1 & \xi & \eta & \xi\eta & 0 & f \end{bmatrix} \tag{42a}$$

$$\underset{\sim}{\beta}^T = \lfloor \beta_1, \beta_2, \ldots\ldots, \beta_{10} \rfloor \tag{42b}$$

In Eqs. (40a) and (42a), f and g represent higher order terms in ξ and η which we will discuss shortly.

It should be pointed out that, for rectangular element shape, the conventional mixed formulation element without f and g terms requires 2 X 2 point rule for exact integration of element stiffness matrix. Then the resulting element is equivalent to the conventional assumed displacement model with 2 X 2 point reduced integration. This equivalence holds because the number of integration points is the same as the number of strain parameters in each component of the

assumed strain field and thus it is possible to set $\underset{\sim}{\varepsilon} = \overline{\underset{\sim}{\varepsilon}}$, $\underset{\sim}{\kappa} = \overline{\underset{\sim}{\kappa}}$ and $\chi = \overline{\chi}$ at the integration points [13,14].

Note that a nine node element without f and g terms in Eqs. (40a) and (42a) will exhibit kinematic modes or spurious zero strain energy modes. For a flat square element with sides along $x = \pm 1$ and $y = \pm 1$ lines, these kinematic modes are as follows [5,15]:

$$(1) \quad u = c_1 \, x \, (1 - 3y^2)$$

$$v = - c_1 \, y \, (1 - 3x^2) \tag{43a}$$

$$(2) \quad u = c_2 \, (x^2 + y^2 - 3x^2y^2) \tag{43b}$$

$$(3) \quad v = c_3 \, (x^2 + y^2 - 3x^2y^2) \tag{43c}$$

$$(4) \quad w = c_4 \, (x^2 + y^2 - 3x^2y^2) \tag{43d}$$

$$(5) \quad \theta_1 = c_5 \, x \, (1 - 3y^2)$$

$$\theta_2 = - c_5 \, y(1 - 3x^2) \tag{43e}$$

$$(6) \quad \theta_1 = c_6 \, (x^2 + y^2 - 3x^2y^2) \tag{43f}$$

$$(7) \quad \theta_2 = c_7 \, (x^2 + y^2 - 3x^2y^2) \tag{43g}$$

where $c_1, \ldots, c_7$ are arbitrary constants. Among all these kinematic modes the modes of Eqs. (43a) and (43e) disappear for an assembly of only two elements. However, all other modes are compatible or commutable and they may result in an unstable finite element model even after assembly of elements. Therefore the higher order terms f and g in $\underset{\sim}{P}_e$, $\underset{\sim}{P}_\kappa$ or $\underset{\sim}{P}_\gamma$ must be chosen appropriately to suppress these undesirable kinematic modes. For example, from Eqs. (43b) and (43c)

$$\frac{\partial u}{\partial x} = C_2(2x-6xy^2)$$

$$\frac{\partial v}{\partial y} = C_3(2y-6x^2y) \tag{44}$$

Then the kinematic modes in Eqs. (43b) and (43c) will disappear if xy^2 and x^2y

terms are added to the bilinear assumed strains ε_{xx} and ε_{xy} respectively. Following the same argument, the xy^2, x^2y terms can be added to the bilinear assumed $\underset{\sim}{\kappa}$ and $\underset{\sim}{\gamma}$ to suppress the spurious modes in Eqs. (43d), (43f) and (43g). Based on this observation, for an element with arbitrary geometry, we choose f and g as follows:

(1) if x is parallel with ξ as in Eq. (36a)

$$f = \xi\eta^2$$

$$g = \xi^2\eta \tag{45a}$$

(2) if x is parallel with η as in Eq. (36b)

$$f = \xi^2\eta$$

$$g = \xi\eta^2 \tag{45b}$$

Table 1 shows the size of $\underset{\sim}{G}_e$, $\underset{\sim}{G}_\kappa$, $\underset{\sim}{G}_\gamma$, $\underset{\sim}{H}_e$, $\underset{\sim}{H}_\kappa$, $\underset{\sim}{H}_\gamma$ matrices which appear in Eqs. (15a) to (15f) for the conventional mixed formulation I. These matrices are evaluated by 3 X 3 point integration rule. Due to the need to evaluate these matrices and invert $\underset{\sim}{H}_e$, $\underset{\sim}{H}_\kappa$ and $\underset{\sim}{H}_\gamma$, the conventional mixed formulation I needs more computing time to generate an element stiffness matrix than the corresponding displacement model based on the principle of virtual work. For the conventional mixed formulation II based on the modified Hellinger-Reissner principle with $\underset{\sim}{\kappa} = \overline{\underset{\sim}{\kappa}}$, it is not necessary to evaluate $\underset{\sim}{G}_\kappa$, $\underset{\sim}{H}_\kappa$ and $\underset{\sim}{H}^{-1}$. In this formulation, the bending stiffness matrix is calculated in the same manner as in the case of assumed displacement model [15]. In the reference 15, a nine node element has been developed based on the conventional formulation II using the same assumed inplane strain and transverse shear strain as in Eq. (40) and (42). Since assumed $\underset{\sim}{\kappa}$ has nothing to do with locking, the property of the resulting element stiffness matrix is nearly identical to that of the conventional formulation I element. Therefore both conventional formulation elements will be collectively designated as SHEL9.

On the other hand, in the new formulation, we set $\underset{\sim}{\varepsilon}_L = \overline{\underset{\sim}{\varepsilon}}$, $\underset{\sim}{\kappa}_L = \overline{\underset{\sim}{\kappa}}$, $\chi = \overline{\chi}$ by by adopting 2x2 point rule and a bilinear function for N_i in Eqs. (21a-c) for the terms involving lower order integrations. For higher order integration, 3 X 3 point rule is used. Then the $\underset{\sim}{K}_L$ matrix in Eq. (31) is exactly the same as the stiffness matrix based on the assumed displacement model with 2x2 point rule. Therefore it has the same kinematic modes given in Eqs. (43a) to (43g). In order to eliminate compatible or commutable modes, we choose the higher order inplane strain as follows:

$$\underset{\sim}{\varepsilon}_H = \overline{\underset{\sim}{P}}_e \underset{\sim}{\alpha} \tag{46}$$

where

$$\overline{\underset{\sim}{P}}_e = \begin{bmatrix} f & 0 \\ 0 & g \\ 0 & 0 \end{bmatrix} \tag{46a}$$

$$\underset{\sim}{\alpha}^T = \lfloor \alpha_1, \alpha_2 \rfloor \tag{46b}$$

For transverse shear strain,

$$\chi_H = \overline{\underset{\sim}{P}}_\gamma \underset{\sim}{\beta} \tag{47}$$

in which

$$\overline{\underset{\sim}{P}}_\gamma = \begin{bmatrix} g & 0 \\ 0 & f \end{bmatrix} \tag{47a}$$

$$\underset{\sim}{\beta}^T = \lfloor \beta_1, \beta_2 \rfloor \tag{47b}$$

In addition, the higher order $\underset{\sim}{\kappa}_H$ is assumed to have the same strain shape function matrix as the higher order assumed inplane strain such that

$$\underset{\sim}{\kappa}_H = \overline{\underset{\sim}{P}}_\kappa \underset{\sim}{\beta}_\kappa \tag{48}$$

where

$$\overline{\underset{\sim}{P}}_\kappa = \overline{\underset{\sim}{P}}_e \tag{48a}$$

$$\underset{\sim}{\beta}_\kappa^T = \lfloor \beta_{\kappa 1}, \beta_{\kappa 2} \rfloor \tag{48b}$$

Note that the higher order assumed independent strain shape function matrices in Eqs. (46a) and (47a) are taken from the last two columns of $\underset{\sim}{P}_e$ and $\underset{\sim}{P}_\gamma$ matrices in Eqs. (40a) and (42a) of the conventional formulation.

The size of $\overline{\underset{\sim}{G}}_e$, $\overline{\underset{\sim}{G}}_\kappa$, $\overline{\underset{\sim}{G}}_\gamma$, $\overline{\underset{\sim}{H}}_e$, $\overline{\underset{\sim}{H}}_\kappa$, $\overline{\underset{\sim}{H}}_\gamma$ matrices in Eqs. (25) to (27) are also listed in table 1. Due to the small size of these matrices as compared with those needed in the conventional formulation, the present new formulation will require less computing time for the generation of an element stiffness matrix than the conventional formulation. In addition, to save computing time, B_e, B_κ, B_γ and $|J|$ at 2 X 2 points are interpolated from $\underset{\sim}{B}_e$, $\underset{\sim}{B}_\kappa$, $\underset{\sim}{B}_\gamma$ and $|\underset{\sim}{J}|$ evaluated at 3 X 3 points as shown in Eqs. (32a-d).

NUMERICAL TESTS

Simple example problems including both plates and shells were solved to test the performance of the nine node element based on the new formulation. Plate bending problems are useful in that the issue of transverse shear locking can be investigated independently of inplane or membrane locking effect. For the purpose of identification, the new formulation element will be called SHEL9N. Whenever possible, the performance of the SHEL9N element is compared with the SHEL9 element based on the conventional formulation. Numerical results are presented in tabular form so that they can be used as a reference for those who might want to compare their shell elements with the present SHEL 9N element. All examples were computed in double precision arithmatic on the UNIVAC 1100/82 machine at the University of Maryland.

(a) Comparison of Computing Time

In order to evaluate computing efficiency a test was run in which stiffness of single nine node curved element was computed ten times consecutively. It

turns out that the computing time for the new formulation element is about 50% of the conventional formulation I element and 60% of the conventional formulation II element. Clearly the new formulation requires less computing time.

(b) Simply Supported or Clamped Square Plate

A quarter of a simply supported or clamped square plate subjected to a uniformly distributed load p is modeled by 2 X 2, 3 X 3 and 4 X 4 meshes. Both evenly divided regular and distorted meshes are considered to investigate the effects of element geometry and boundary conditions on the element. The three distorted meshes are illustrated in Fig. 3. Elastic properties of the plate are $E = 10^7$ psi and $\nu = 0.3$. Tables 2 and 3 show the nondimensional maximum deflection at the centroid of the plate for uniform regular mesh. The computed values are normalized with respect to the analytical solutions at the plate centroid obtained from thin plate theory [18]. The results of distorted meshes are given in Tables 4 and 5. The ratios of plate length to thickness ranges from 10^2 to 10^5. The numerical values of SHEL9 are taken from reference 15. The results for 3 X 3 meshes are not reported in this reference. All numerical results for uniform regular meshes are very close to the exact solution and are insensitive to the wide range of L/t ratios. Also there is virtually no difference between SHEL9N and SHEL9 elements. For distorted meshes, solutions of both models are slightly less accurate than those for uniform regular meshes, and the performance of both elements decreases as the plate becomes thin, especially for the clamped plate. However, values of L/t over 10^3 are beyond a practical range.

Table 6 lists the nondimensional maximum bending moment for the uniform regular meshes evaluated at the integration point nearest to the centroid of the plate. The computed values are normalized with respect to the analytical solution at the plate centroid obtained from thin plate theory. Note that for the

conventional mixed element, the moment is computed at 3 X 3 integration points while, for the present new mixed element, the moment is computed at 2 X 2 integration points. Therefore the sampling point for the conventional mixed element is closer to the centroid than that for the present new mixed model. Again the reliability of both new and conventional mixed elements is evident.

(c) A Circular Plate with Clamped Boundary

A quarter of a circular plate under uniformly distributed load p per unit area is modeled by 8-element, 12-element and 16-element meshes as shown in Fig. 4. The radius R of the circular plate is 5 inches and elastic constants are $E = 10^7$ psi and $\nu = 0.3$.

The computed maximum nondimensional deflection $\bar{w}_0 = 64\ Dw/pR^4$ at the plate centroid is listed in Table 7. The analytical solution obtained from the classical thin plate theory is $\bar{w}_0 = 1.0$. The numerical result in Table 7 shows that the present SHEL9N element is as reliable as the SHEL9 element based on the conventional mixed formulation. Both elements are free of shear locking and give accurate solutions, especially for the 16-element model. It appears that the SHEL9N element solution is slightly more accurate than the SHEL9 solution. However the difference is very small.

(d) A Pinched Cylinder with Diaphragmed Ends

A pinched cylinder with diaphragmed ends has been frequently used as a deep shell example because an analytical solution is available for comparison. As shown in Fig. 5, a cylindrical shell of length L and radius R is pinched by a concentrated load P at two opposite points on the circle of the middle section. Due to the symmetry in geometry and loading, only one eighth of the cylindrical shell is modeled by 6 X 4, 7 X 5, 8 X 6, 8 X 6F, 9 X 7 and 9 X 7F meshes. As an example, the 9 X 7 and 9 X 7F meshes are depicted in Fig. 6. The 8 X 6F and 9 X 7F meshes are obtained from 7 X 5 and 8 X 6 uniform meshes respectively by dividing the strips along the lines BC and CD equally. These refined meshes are

used to model the steep gradients of deflections and stresses in the region of the concentrated load point C. Material and geometric data are $E = 1.05 \times 10^7$ psi, $\nu = 0.3$, $R = 4.953$ in., $L = 2R$ and $R/t = 100, 300, 500$.

The nondimensional displacements $\bar{w}_c = -w_c Et/P$ at the load point C are listed in Table 8 for both SHEL9N and SHEL9 elements together with analytical solutions. Analytical solutions were calculated by taking 100 terms in each direction for a double Fourier series expression as given in reference 19. In reference 15, the 9 X 7 mesh was not tested. This table shows that both mixed models work very well for this deep shell problem. Even though SHEL9N has a slight edge over the SHEL9 model, the differences are negligible. For the case of $R/t = 100$, the converged value of $\bar{w}_c$ is higher than the analytical solution obtained by the thin shell theory which neglects transverse shear effect. In Fig. 7, the distribution of nondimensional deflection along the arc BC for 9 X 7F mesh is compared for different R/t ratios. Note that curves for higher R/t ratios have steep gradients near point C. This means that more elements and finer meshes are required to model the region near the concentrated load P in order to obtain accurate results. More numerical results are given in reference 20.

(e) A Pinched Spherical Shell

A pinched spherical shell shown in Fig. 8 serves as another example of deep shells. The spherical shell is a doubly curved shell in contrast to the singly curved cylindrical shell. The implementation of finite element analysis, however, is relatively simple due to the symmetry in geometry and loading. In addition, an analytical solution is available [21]. Due to symmetry in shell geometry and loading conditions, only a 2^o segment of the upper half sphere is modeled by four different meshes of the SHEL9N elements. The segment angles of elements in different meshes are listed in Table 9. The region at the loading point is modeled by one six-node triangular mixed formulation element [22] with

linear distribution of assumed inplane and transverse shear strain fields.

Elastic properties and shell geometry are $E = 10^7$ psi, $\nu = 0.3$, $t = 1$ in. and $R/t = 50, 100, 500, 1000$. Table 10 compares the nondimensional normal deflection $\bar{w} = Etw/P$ at the pole. For $R/t = 500$ and 1000, the agreement between numerical results and analytical solution is very good. For lower R/t ratios, the differences are slightly larger. In fact, for these ratios the transverse shear effect may not be negligile. Note that Koiter's analytical solution is based on thin shell theory which neglects the effect of transverse shear strain. Figure 9 represents the nondimensional normal deflection of the 18-element mesh. The steep gradient near the pole is observed for very high R/t ratios. More numerical results can be found in reference 20.

CONCLUSIONS

Numerical test shows that, in terms of computing time, the new formulation is more efficient than the conventional mixed formulation. In fact the computing time for the new SHEL9N element stiffness matrix is about half of that for the element based on the conventional formulation.

The SHEL9N element is free of locking and undesirable compatible or commutable kinematic modes as is the SHEL9 element based on a conventional mixed formulation. In fact, the stiffness matrix associated with the higher order assumed strain plays the role of a stabilization matrix.

The SHEL9N element provides very accurate solutions for thin plates and shells. Therefore, we recommend it be included in general purpose finite element programs.

ACKNOWLEDGEMENT

The present work was supported by the Office of Naval Research (N00014-84-K-0385).

REFERENCES

1. S. Ahmad, B.M. Irons and O.C. Zienkiewicz, "Analysis of Thick and Thin Shell Structures by Curved Elements," Int. J. Num. Meth. Engn., 2, 419-451 (1970).

2. S.W. Lee and T.H.H. Pian, "Improvement of Plate and Shell Finite Elements by Mixed Formulations," AIAA J., 16, 29-34 (1978).

3. O.C. Zienkiewicz, J. Too and R.L. Taylor, "Reducd Integration Technique in General Analysis of Plates and Shells," Int. J. Num. Meth. Engng., 3, 275-290 (1971).

4. S.F. Pawsey and R.W. Clough, "Improved Numerical Integration of Thick Shell Finite Elements," Int. J. Num. Meth. Engng., 3, 575-586 (1971).

5. T.J.R. Hughes, M. Cohen and M. Haroun, "Reduced and Selective Integration Techniques in the Finite Analysis of Plates," Nuclear Engng. Design, 46, 203-222 (1978).

6. E.D.L. Pugh, E. Hinton and O.C. Zienkiewicz, "A Study of Quadrilateral Plate Bending Elements with Reduced Integration," Int. J. Num. Meth. Engng., 12, 1059-1079 (1978).

7. H. Stolarski and T. Belytschko, "Membrane Locking and Reduced Integration for Curved Elements," J. of Applied Mechanics, 49, 172-176 (1982).

8. T.J.R. Hughes, R.L. Taylor and W. Kanoknukulchai, "A Simple and Efficient Finite Element for Plate Bending," Int. J. Num. Meth. Engng., 11, 1529-1543 (1977).

9. H. Parish, "A Critical Survey of the 9-Node Degenerated Shell Element with Special Emphasis on Thin Shell Application and Reduced Integration," Comp. Meths. Appl. Mech. Engng., 20, 323-350 (1979).

10. N. Bicanic and E. Hinton, "Spurious Modes in Two-Dimensional Isoparametric Elements," Int. J. Num. Meth. Engng., 14, 1545-1557 (1979).

11. T. Belytschko, J.S.J. Ong and W.K. Liu, "A Consistent Control of Spurious Singular Modes in the 9-Node Lagrange Element for the Laplace and Mindlin Plate Equations," Comp. Meth. App. Mech. Engng., 44, 269-295 (1984).

12. T. Belytschko, W.K. Liu, J.S.J. Ong and D. Lam, "Implementation and Application of a 9-node Lagrangian Shell Element with Spurious Mode Control," Computers and Structures, 20, 121-128 (1985).

13. S.W. Lee, "Finite Element Methods for Reduction of Constraints and Creep Analysis," Ph.D. dissertation, Dept. Aero. and Astro., MIT, Feb. (1978).

14. D.S. Malkus and T.J.R. Hughes, "Mixed Finite Element Methods - Reduced and Selective Integration Techniques: A Unification of Concepts," Comp. Meths. Appl. Mech. Engng., 15, 63-81 (1978).

15. S.C. Wong, "A Nine Node Assumed Strain Finite Element Model for Analysis of Thin Shell Structures," Ph.D. dissertation, Dept. of Aero. Engng., University of Maryland, May 1985.

16. S.W. Lee, S.C. Wong and J.J. Rhiu, "Study of a Nine-Node Mixed Formulation Finite Element for Thin Plates and Shells," Computers and Structures, 21, 1325-1334, (1985).

17. S.W. Lee and J.J. Rhiu, "A New Efficient Approach to the Formulation of Mixed Finite Element Models for Structural Analysis," accepted for publication in Int. J. Num. Meth. Engng. (1986).

18. S.P. Timoshenko and S. Woinowsky-Krieger, Theory of Plate and Shells, 2nd Ed., McGraw-Hill, New York, 1959.

19. W. Flugge, Stresses in Shells, Springer-Verlag, Berlin, 1962.

20. J.J. Rhiu, "A New and Efficient Formulation for Finite Element Analysis of Thin Shell Structures Undergoing Small and Large Deflection," Ph.D. dissertation, Dept. of Aero. Engng., University of Maryland, Aug. 1985.

21. W.T. Koiter, "A Spherical Shell under Point Loads at Its Pole," Progress in Appl. Mech., the Prager Anniversary Volume, 155-169, MacMillan, 1963.

22. S.W. Lee, C.C. Dai and C.H. Yeom, "A Triangular Finite Element for Thin Plates and Shells," Int. J. Num. Meth. Engng., 21, 1813-1831 (1985).

Table 1. Matrix size of the nine node shell element

Matrix	Conventional Formulation I	Conventional Formulation II	Matrix	New Formulation
$\underset{\sim}{G}_e$	14 X 45	14 X 45	$\overline{\underset{\sim}{G}}_e$	2 X 45
$\underset{\sim}{G}_\kappa$	14 X 45	—	$\overline{\underset{\sim}{G}}_\kappa$	2 X 45
$\underset{\sim}{G}_\gamma$	10 X 45	10 X 45	$\overline{\underset{\sim}{G}}_\gamma$	2 X 45
$\underset{\sim}{H}_e$	14 X 14	14 X 14	$\overline{\underset{\sim}{H}}_e$	2 X 2
$\underset{\sim}{H}_\kappa$	14 X 14	—	$\overline{\underset{\sim}{H}}_\kappa$	2 X 2
$\underset{\sim}{H}_\gamma$	10 X 10	10 X 10	$\overline{\underset{\sim}{H}}_\gamma$	2 X 2

Table 2. Nondimensional maximum deflection of simply supported square plate under uniformly distributed pressure (uniform regular meshes)

L/t	Type	2 X 2	3 X 3	4 X 4
10^2	SHEL9N SHEL9	1.0027 1.0023	1.0010 ——	1.0007 1.0007
10^3	SHEL9N SHEL9	1.0022 1.0017	1.0005 ——	1.0002 1.0002
10^4	SHEL9N SHEL9	1.0022 1.0017	1.0005 ——	1.0002 1.0002
10^5	SHEL9N SHEL9	1.0022 1.0017	1.0005 ——	1.0002 1.0002

Table 3. Nondimensional maximum deflection of clamped square plate under uniformly distributed pressure (uniform regular mesh)

L/t	Type	2 X 2	3 X 3	4 X 4
10^2	SHEL9N SHEL9	1.0134 1.0108	1.0047 ——	1.0032 1.0027
10^3	SHEL9N SHEL9	1.0111 1.0088	1.0024 ——	1.0008 1.0007
10^4	SHEL9N SHEL9	1.0111 1.0088	1.0024 ——	1.0008 1.0007
10^5	SHEL9N SHEL9	1.0111 1.0088	1.0024 ——	1.0008 1.0007

Table 4. Nondimensional maximum deflection of simply supported square plate under a uniformly distributed pressure (distorted meshes)

L/t	Type	2 X 2	3 X 3	4 X 4
10^2	SHEL9N SHEL9	1.0027 0.9992	1.0010 ——	1.0007 1.0004
10^3	SHEL9N SHEL9	0.9902 0.9796	0.9988 ——	1.0000 0.9981
10^4	SHEL9N SHEL9	0.9842 0.9759	0.9953 ——	0.9988 0.9942
10^5	SHEL9N SHEL9	0.9842 0.9758	0.9948 ——	0.9985 0.9939

Table 5. Nondimensional maximum deflection of clamped square plate under uniformly distributed pressure (distorted meshes)

L/t	Type	2 X 2	3 X 3	4 X 4
10^2	SHEL9N SHEL9	1.0111 0.9974	1.0040 ——	1.0024 0.9982
10^3	SHEL9N SHEL9	0.9186 0.9751	0.9755 ——	0.9960 0.9819
10^4	SHEL9N SHEL9	0.8530 0.9820	0.9447 ——	0.9747 0.9795
10^5	SHEL9N SHEL9	0.8490 0.8838	0.9407 ——	0.9715 0.9678

Table 6. Nondimensional bending moments M_{xx} at the integration point nearest to the centroid of square plate under uniformly distributed pressure (4 X 4 regular mesh)

L/t	Type	Simply Supported	Clamped
10^2	SHEL9N SHEL9	0.9951 1.0008	0.9908 1.0011
10^3	SHEL9N SHEL9	0.9951 1.0008	0.9907 1.0012
10^4	SHEL9N SHEL9	0.9951 1.0008	0.9907 1.0012
10^5	SHEL9N SHEL9	0.9951 1.0008	0.9907 1.0012

Table 7. Nondimensional maximum deflection for circular plate with clamped boundary.

2R/t	Type	Number of elements		
		8	12	16
10^2	SHEL9N	1.0023	1.0014	1.0013
	SHEL9	1.0024	1.0018	1.0015
10^3	SHEL9N	0.9982	0.9948	0.9979
	SHEL9	0.9931	0.9943	0.9974
10^4	SHEL9N	0.9805	0.9822	0.9918
	SHEL9	0.9632	0.9809	0.9906
10^5	SHEL9N	0.9790	0.9810	0.9915
	SHEL9	0.9546	0.9791	0.9901

Table 8. Nondimensional maximum deflection for pinched cylinder with diaphragmed ends

	R/t = 100		R/t = 300		R/t = 500	
Mesh	SHEL9N	SHEL9	SHEL9N	SHEL9	SHEL9N	SHEL9
6X4	164.3	162.4	629.5	619.2	1142.1	1122.5
7X5	164.5	163.2	638.7	630.3	1178.8	1161.9
8X6	165.0	163.8	642.6	635.6	1199.0	1184.3
9X7	165.2	---	644.3	---	1209.5	----
8X6F	165.5	165.0	645.3	642.1	1215.5	1207.3
9X7F	165.7	---	646.4	---	1218.7	----
Flügge [21]	164.3		647.3		1223.4	

Table 9. Segment angles of elements for pinched spherical shell

Type	Number of Elements	Segment angles ($\Delta\phi_i$) in degrees
Mesh 1	9	2,3,5,7,10,15,20,25
Mesh 2	12	1,1,2,2,4,6,6,8,10,15,15,20
Mesh 3	15	0.5,0.5,1,2,2,4,4,6,8,10,10, 10,10,12
Mesh 4	18	0.25,0.5,0.5,0.75,1,2,3,4,4, 6,6,8,8,8,8,10,10,10

Table 10. Nondimensional normal deflection at the pole of pinched sphere

R/t	50	100	500	1000
Mesh 1	23.17	44.17	220.95	445.62
Mesh 2	23.40	44.05	212.67	428.47
Mesh 3	23.71	44.28	209.91	417.61
Mesh 4	24.05	44.60	209.41	415.36
Koiter [21]	21.20	41.93	207.32	413.92

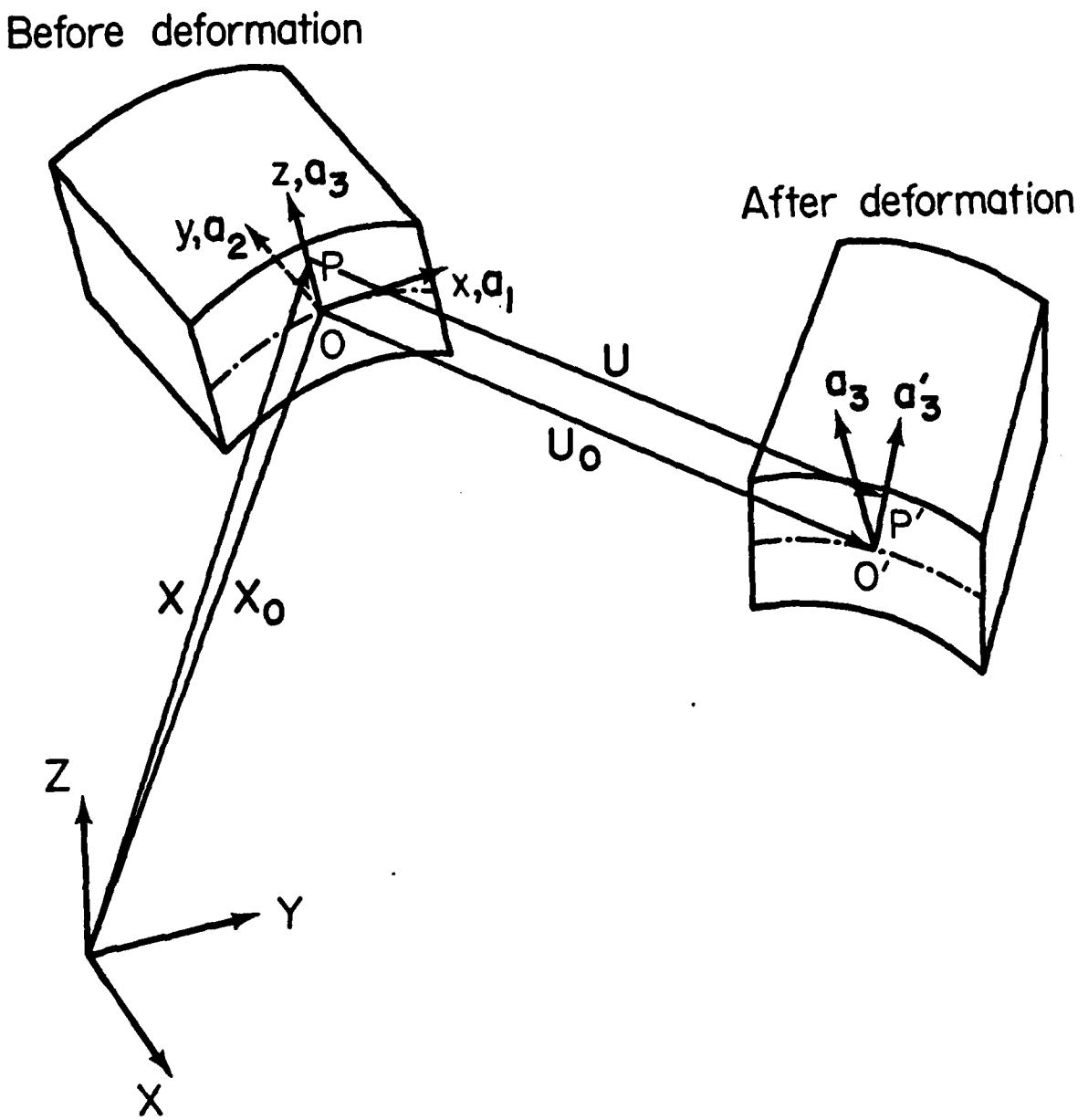

Fig. 1 Kinematics of Shell Motion

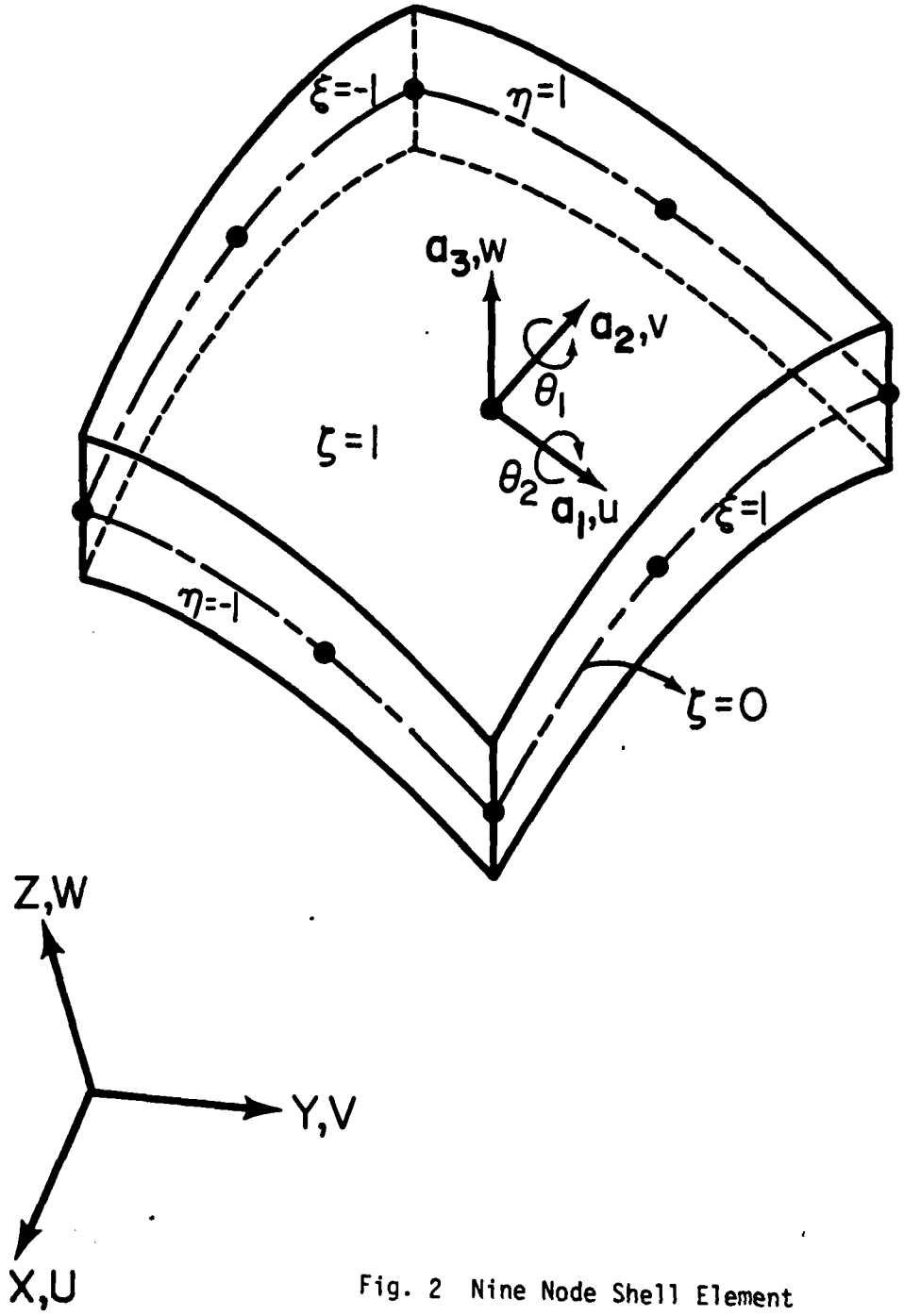

Fig. 2 Nine Node Shell Element

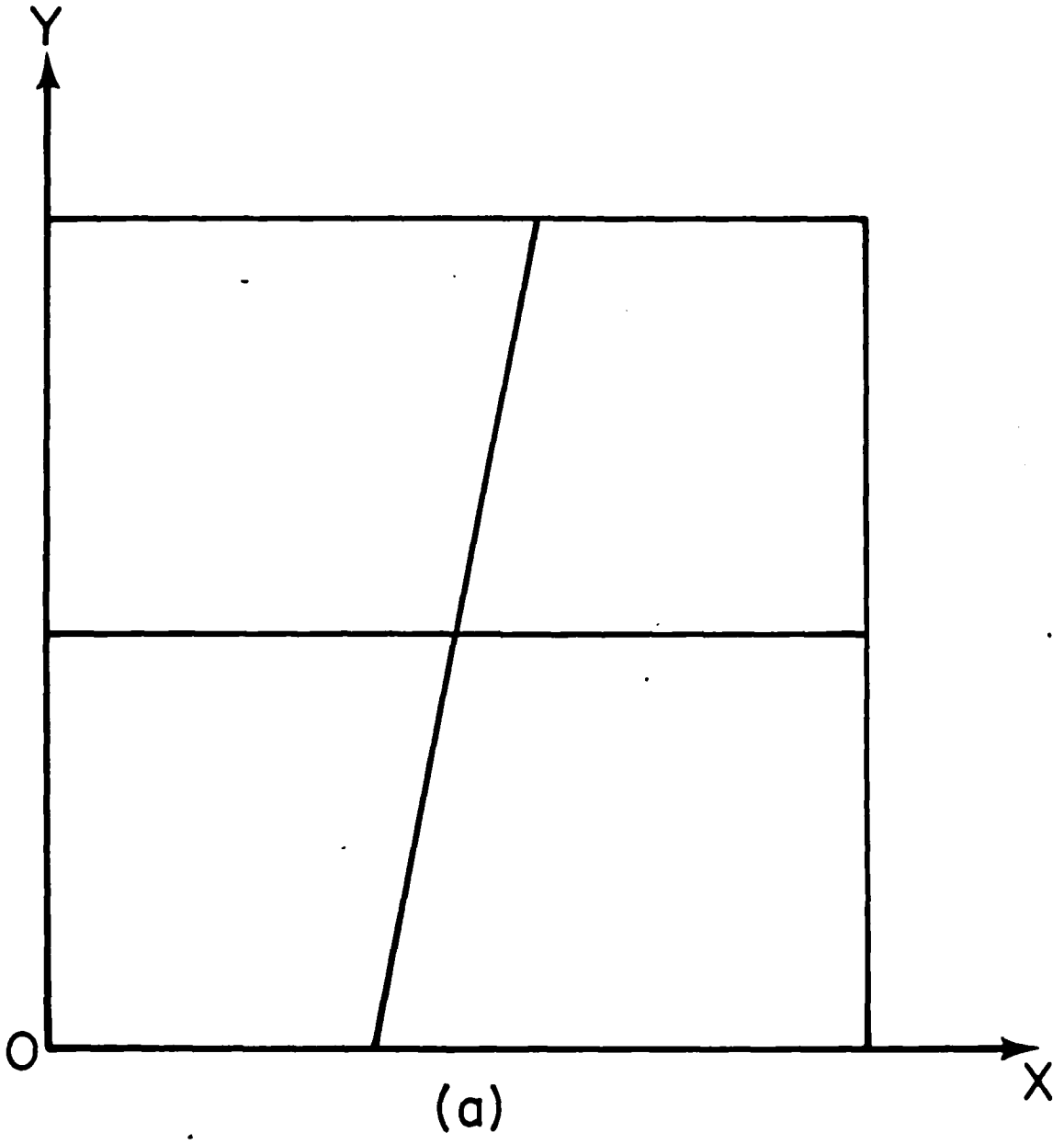

Fig. 3(a) 2x2 Distorted Mesh for a Quarter of Square Plate

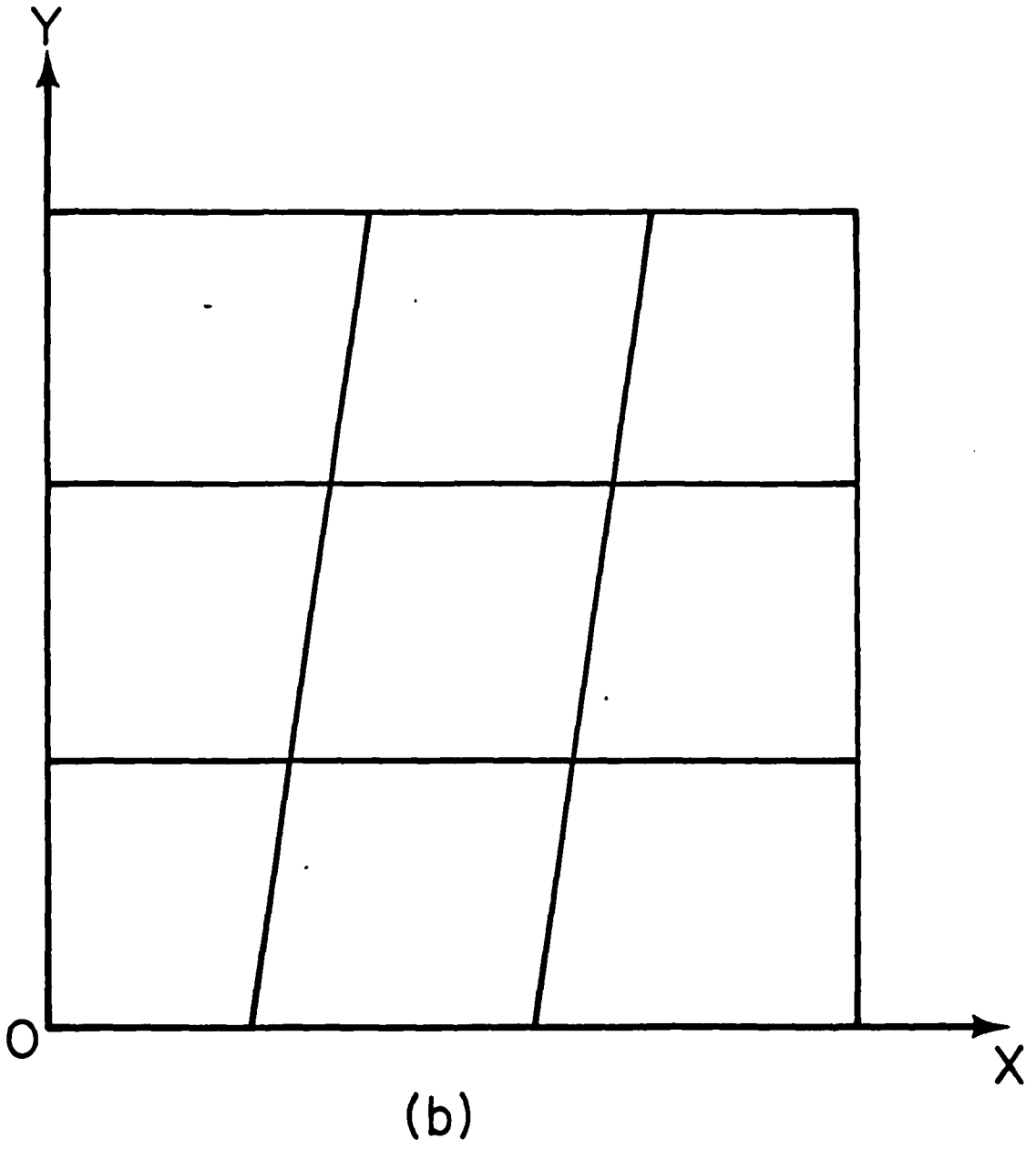

Fig. 3(b) 3x3 Distorted Mesh for a Quarter of Square Plate

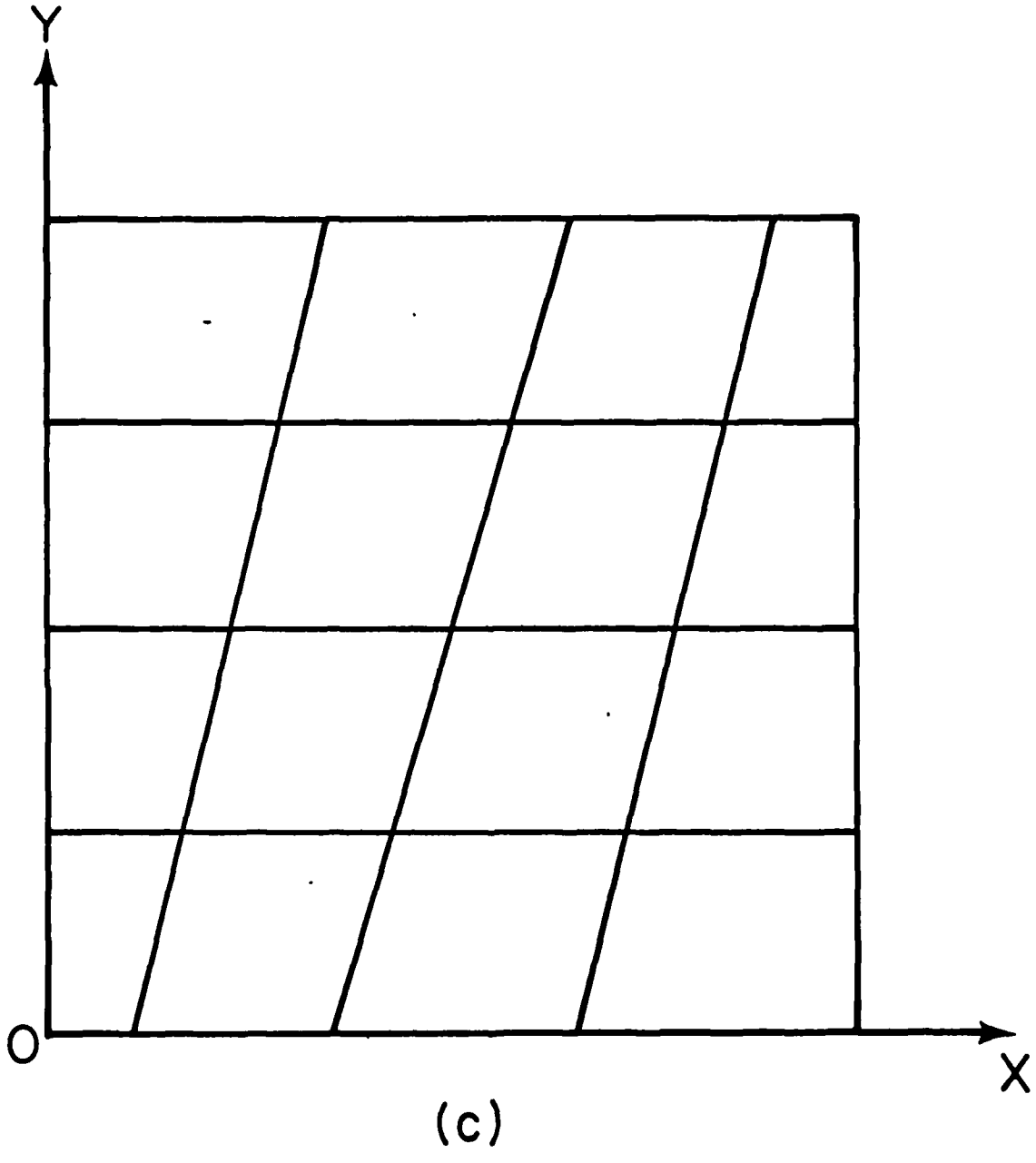

Fig. 3(c) 4x4 Distorted Mesh for a Quarter of Square Plate

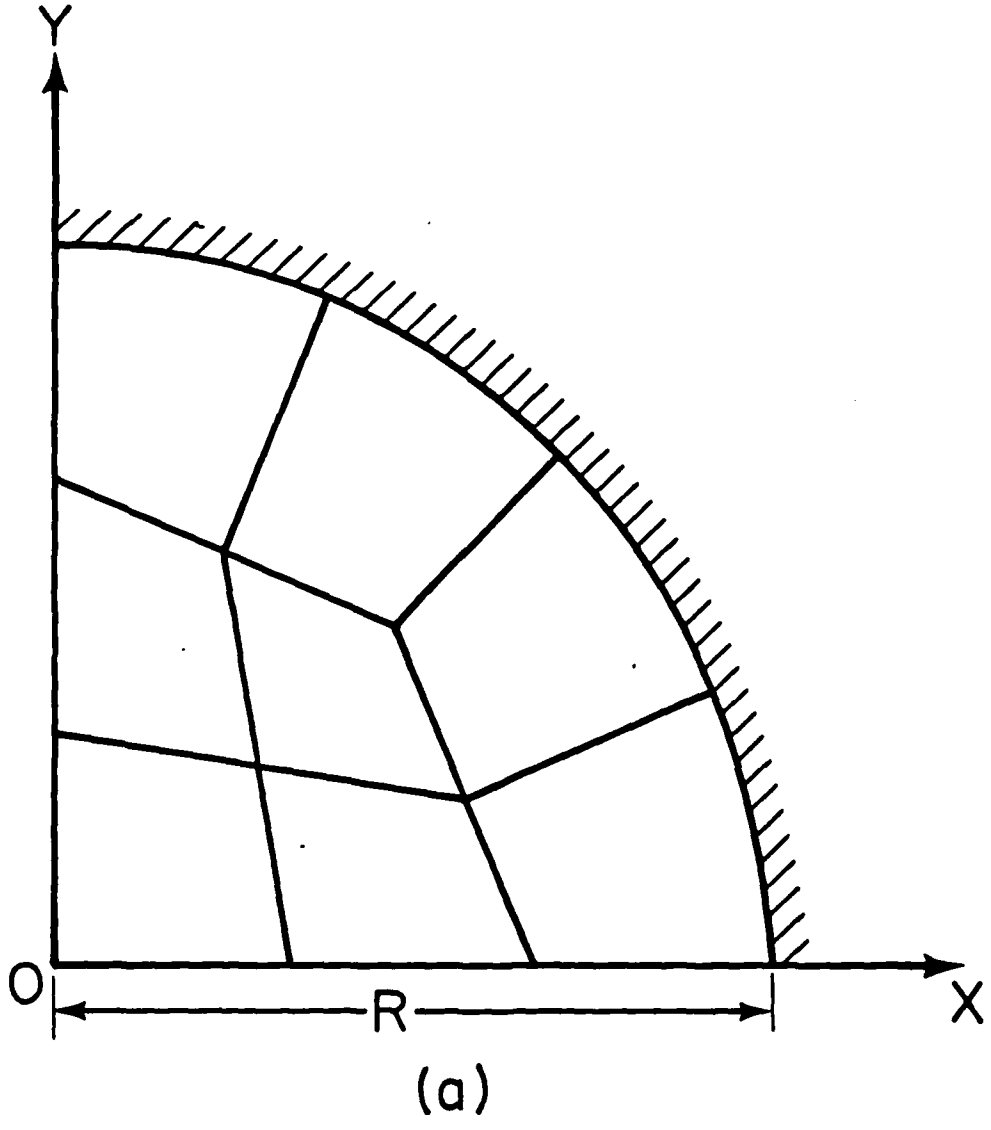

Fig. 4(a) Eight Element Model for a Quarter of a Circular Plate

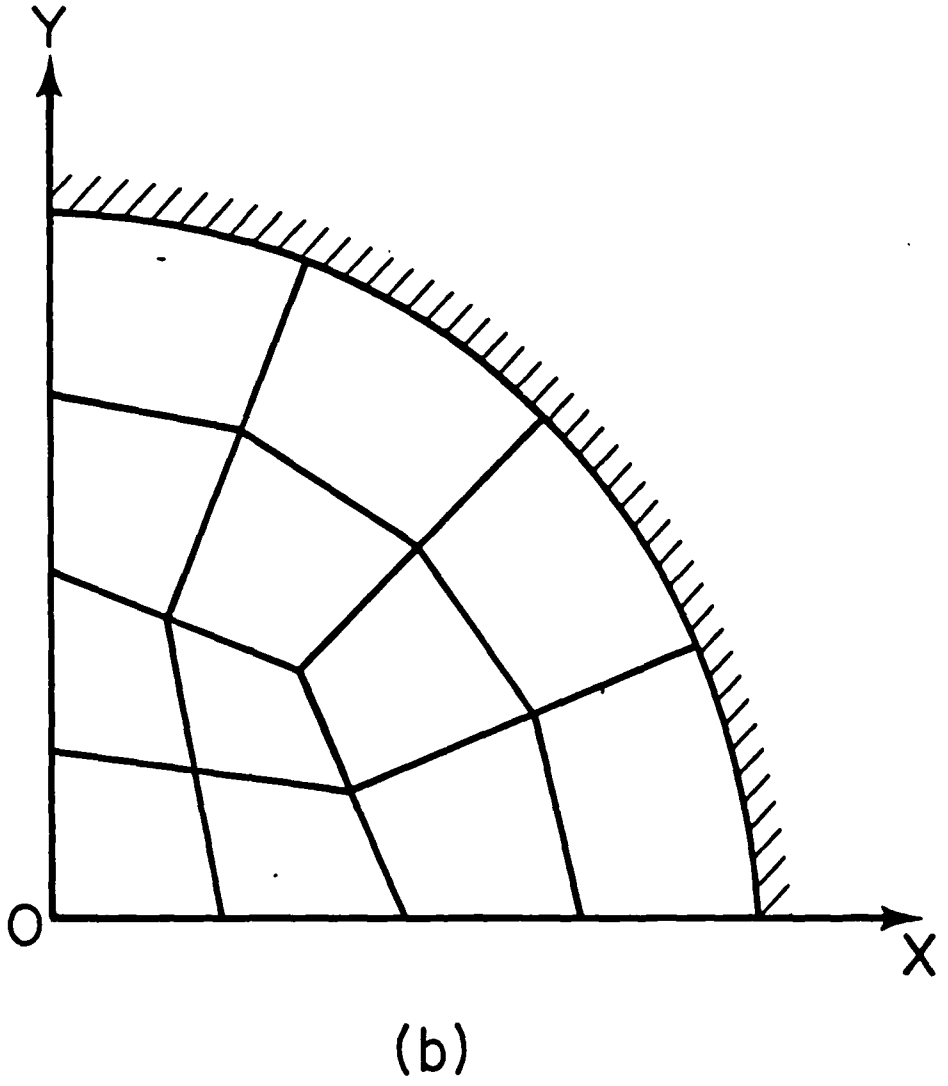

(b)

Fig. 4(b) Twelve Element Model for a Quarter of Circular Plate

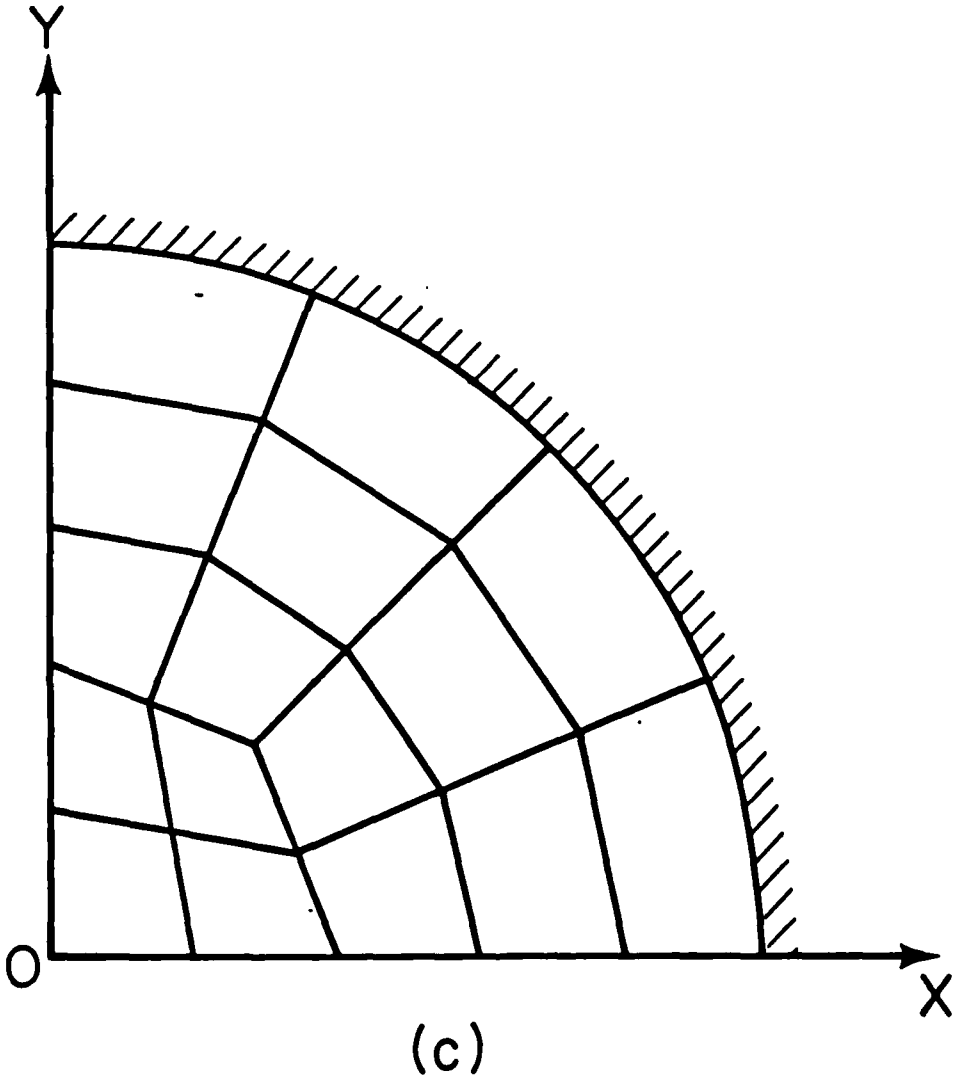

Fig. 4(c) Sixteen Element Model for a Quarter of Circular Plate

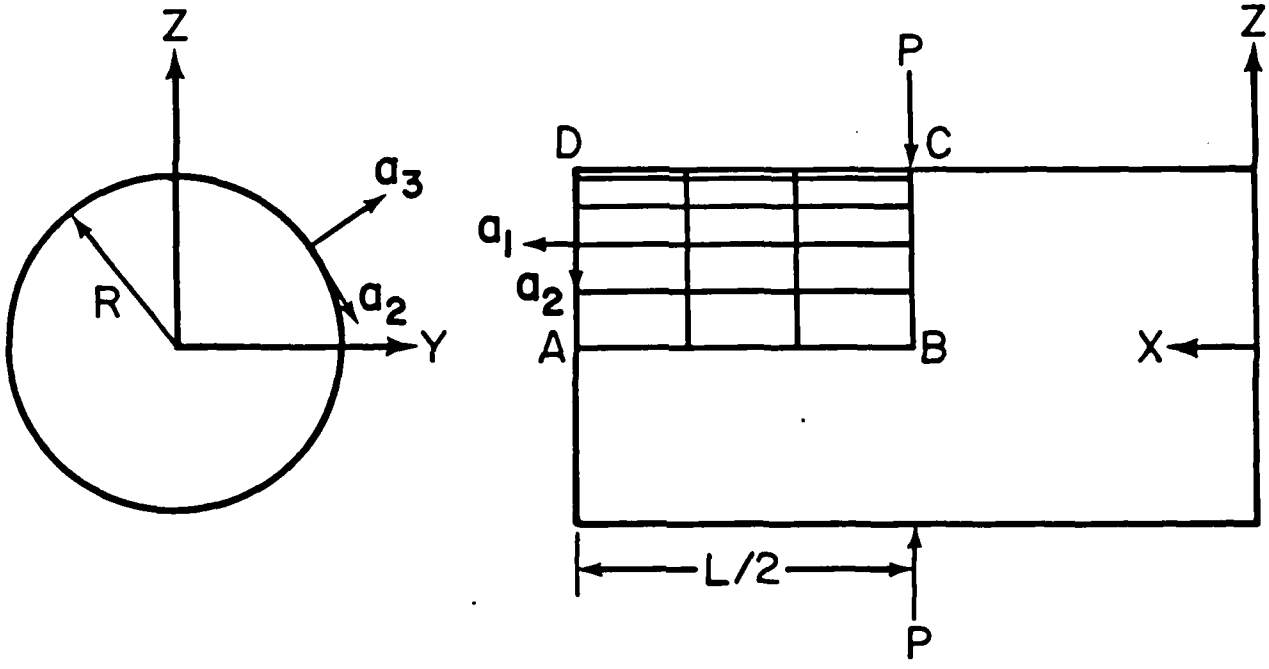

Fig. 5 A Pinched Cylindrical Shell

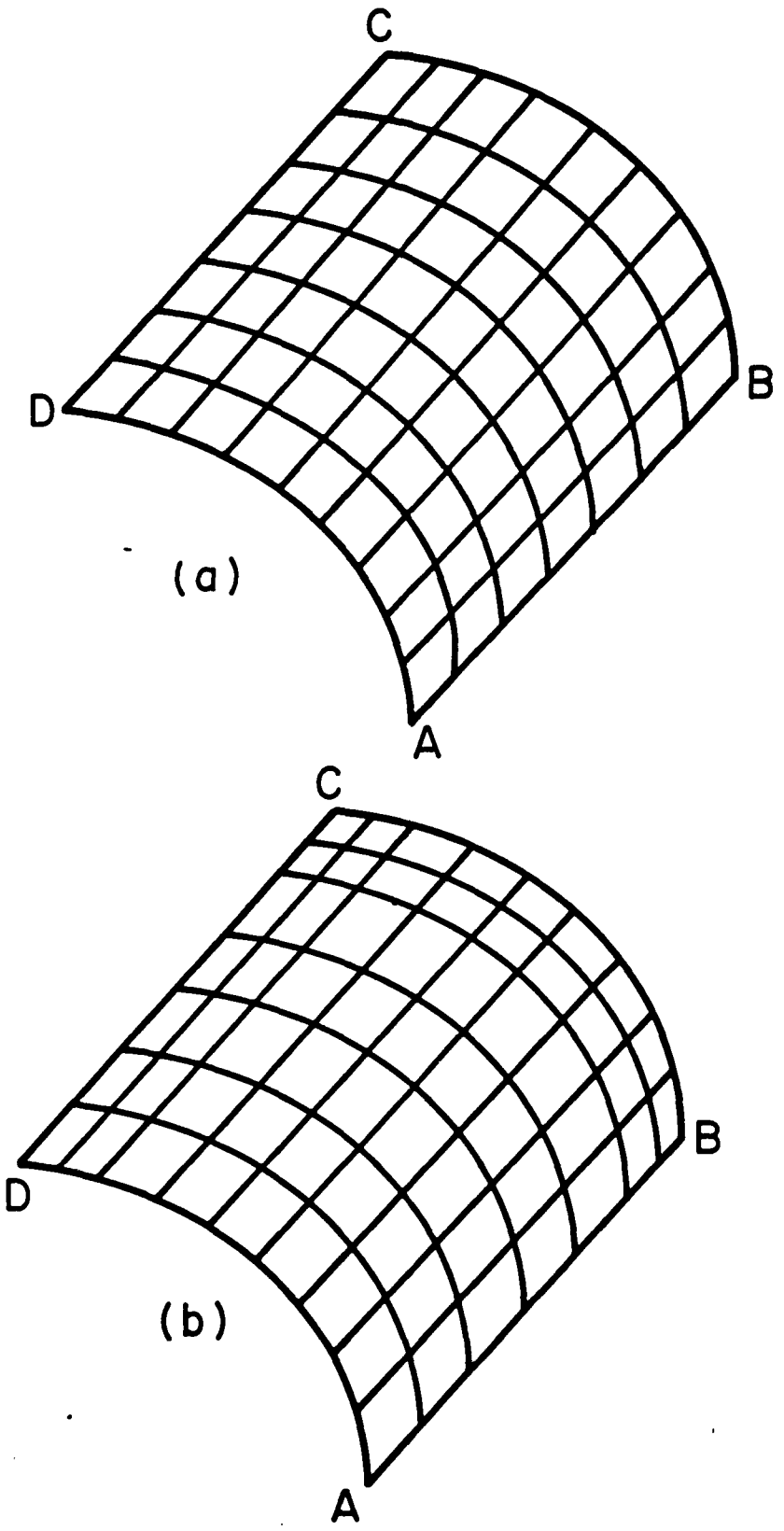

Fig. 6 Finite Element Mesh for an Octant of Cylindrical Shell

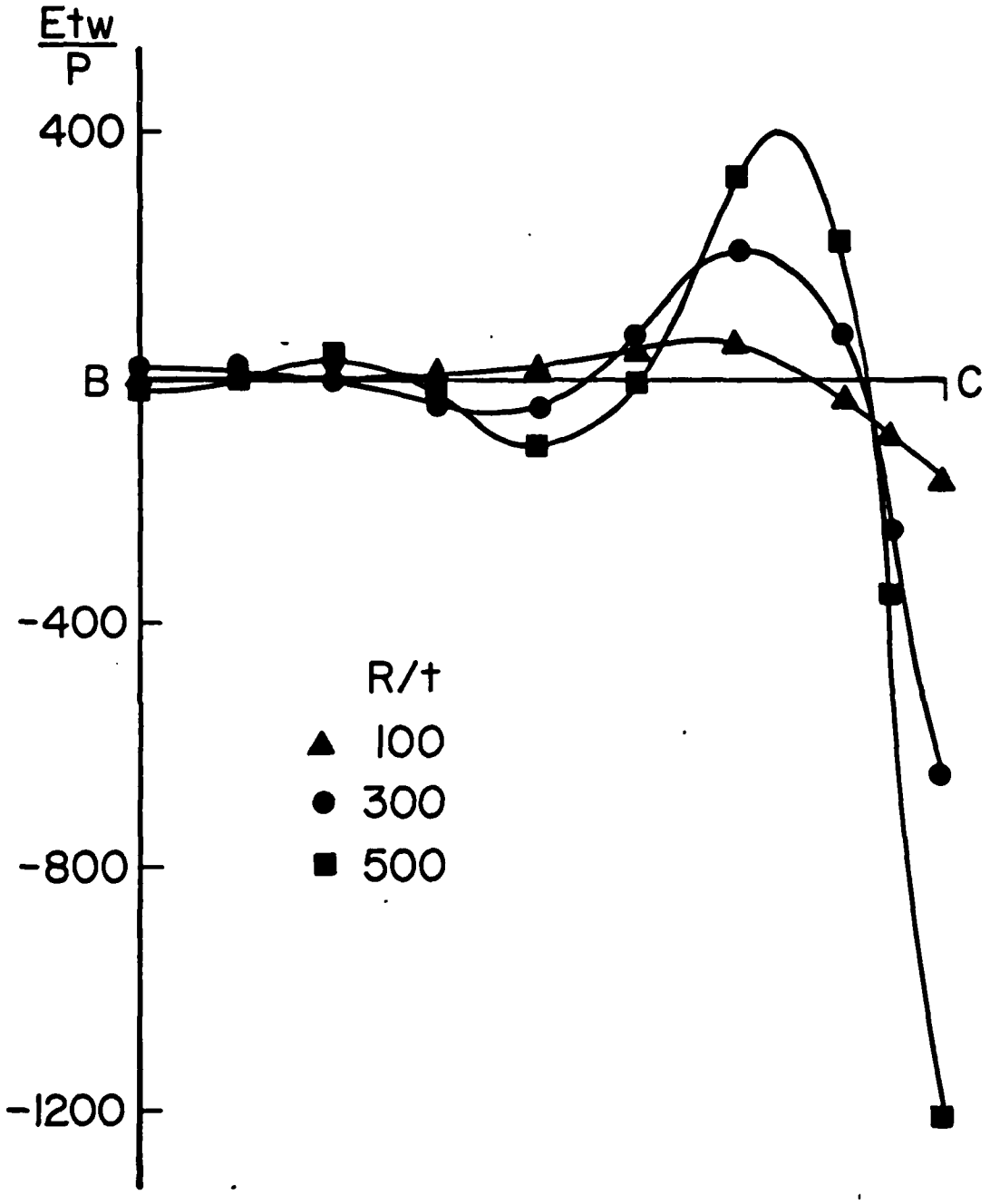

Fig. 7 Nondimensional Deflection along BC for the Cylindrical Shell

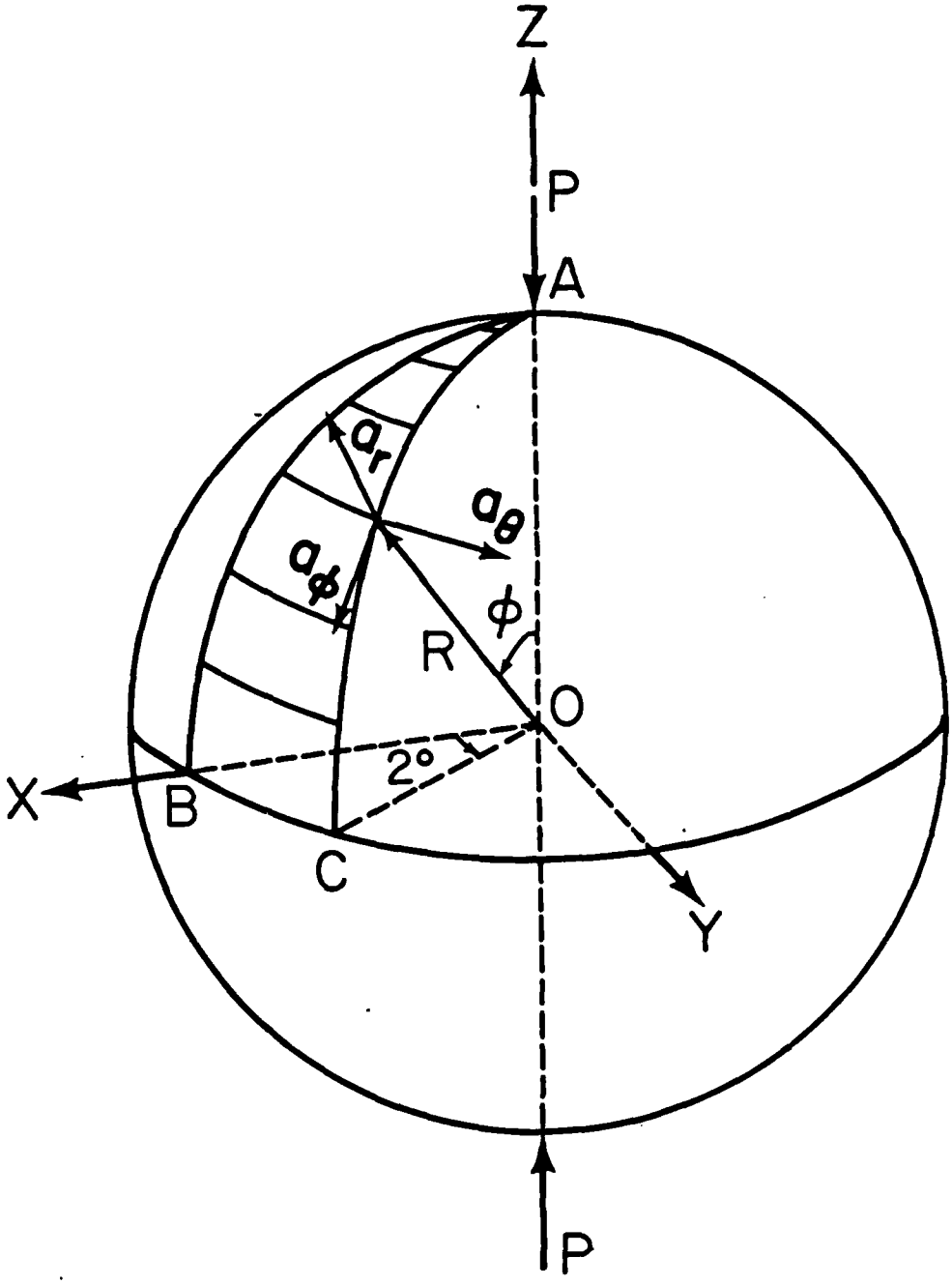

Fig. 8 A Pinched Spherical Shell

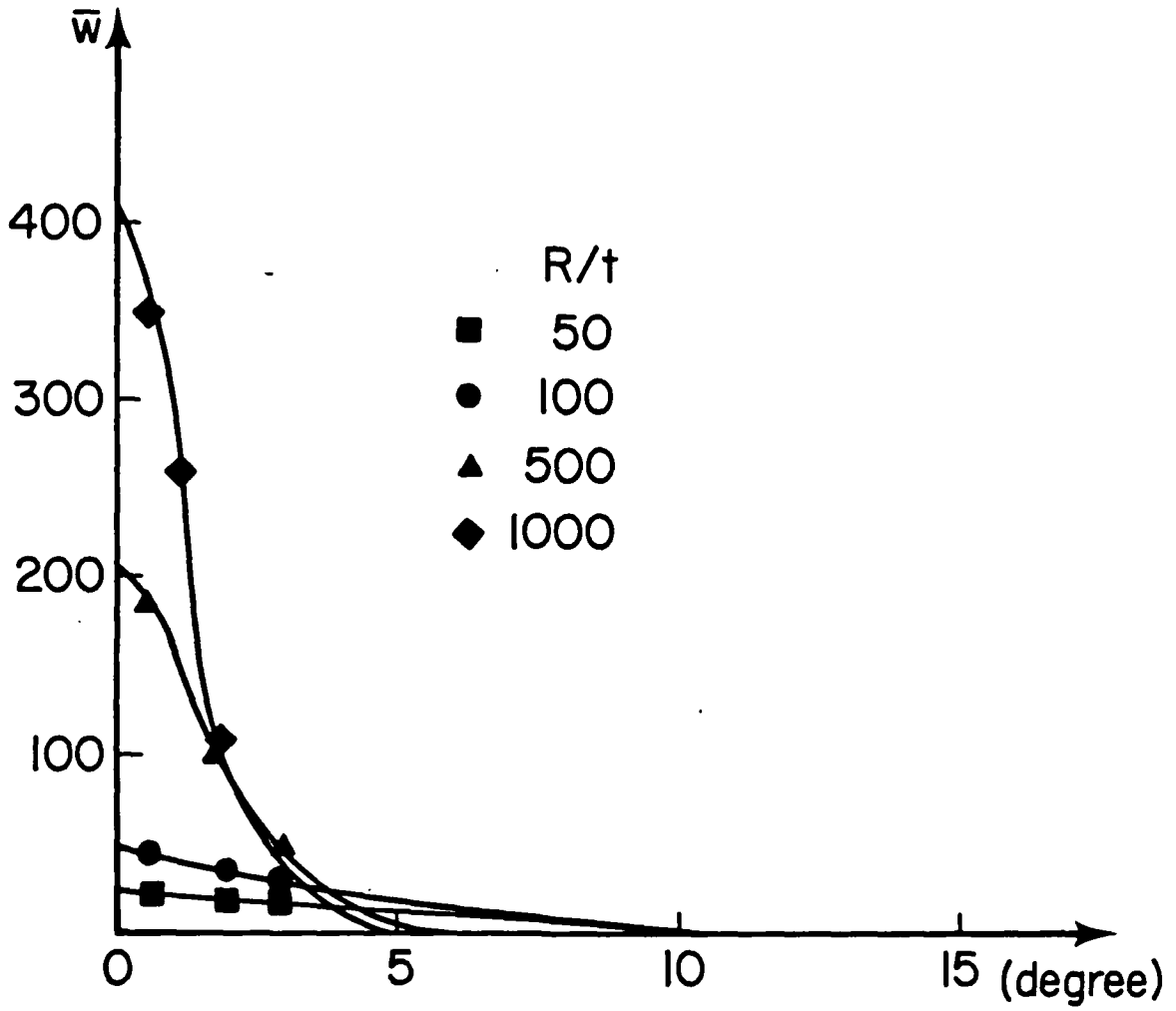

Fig. 9 Normal Deflection along ϕ for the Spherical Shell

END

12-86

DTIC